



HAL
open science

Photocatalytic Deoxygenation of N–O Bonds with Rhenium Complexes: From the Reduction of Nitrous Oxide to Pyridine N-Oxides

Marianne Kjellberg, Alexia Ohleier, Pierre Thuéry, Emmanuel Nicolas, Lucile Anthore-Dalion, Thibault Cantat

► **To cite this version:**

Marianne Kjellberg, Alexia Ohleier, Pierre Thuéry, Emmanuel Nicolas, Lucile Anthore-Dalion, et al.. Photocatalytic Deoxygenation of N–O Bonds with Rhenium Complexes: From the Reduction of Nitrous Oxide to Pyridine N-Oxides. 2021. cea-03277737v1

HAL Id: cea-03277737

<https://cea.hal.science/cea-03277737v1>

Preprint submitted on 13 Apr 2021 (v1), last revised 5 Jul 2021 (v2)

HAL is a multi-disciplinary open access archive for the deposit and dissemination of scientific research documents, whether they are published or not. The documents may come from teaching and research institutions in France or abroad, or from public or private research centers.

L'archive ouverte pluridisciplinaire **HAL**, est destinée au dépôt et à la diffusion de documents scientifiques de niveau recherche, publiés ou non, émanant des établissements d'enseignement et de recherche français ou étrangers, des laboratoires publics ou privés.



Distributed under a Creative Commons Attribution - NonCommercial - NoDerivatives 4.0 International License

Photocatalytic Deoxygenation of N–O Bonds with Rhenium Complexes: From the Reduction of Nitrous Oxide to Pyridine N-Oxides

Marianne Kjellberg, Alexia Ohleier, Pierre Thuéry, Emmanuel Nicolas, Lucile Anthore-Dalton, Thibault Cantat

Submitted date: 08/04/2021 • Posted date: 08/04/2021

Licence: CC BY-NC-ND 4.0

Citation information: Kjellberg, Marianne; Ohleier, Alexia; Thuéry, Pierre; Nicolas, Emmanuel; Anthore-Dalton, Lucile; Cantat, Thibault (2021): Photocatalytic Deoxygenation of N–O Bonds with Rhenium Complexes: From the Reduction of Nitrous Oxide to Pyridine N-Oxides. ChemRxiv. Preprint.

<https://doi.org/10.26434/chemrxiv.14386814.v1>

The accumulation of nitrogen oxides in the environment calls for new pathways to interconvert the various oxidation states of nitrogen, and especially their reduction. The large spectrum of reduction potentials covered by nitrogen oxides makes it however difficult to find general systems capable of efficiently reducing various N-oxides. Here photocatalysis unlocks high energy species able to both circumvent the inherent low reactivity of the greenhouse gas and oxidant N_2O ($E^\circ(\text{N}_2\text{O}/\text{N}_2) = +1.77$ V vs. SHE), and reduce pyridine N-oxides ($E_{1/2}(\text{pyridine N-oxide/pyridine}) = -1.04$ V vs. SHE). The rhenium complex $[\text{Re}(4,4'\text{-tBu-bpy})(\text{CO})_3\text{Cl}]$ proved to be efficient to perform both reactions under ambient conditions, enabling the deoxygenation of N_2O as well as synthetically relevant and functionalized pyridine N-oxides.

File list (4)

text-preprint.pdf (1.17 MiB)

[view on ChemRxiv](#) • [download file](#)

ESI.pdf (2.61 MiB)

[view on ChemRxiv](#) • [download file](#)

Re-4.cif (1.55 MiB)

[view on ChemRxiv](#) • [download file](#)

Re-5.cif (576.06 KiB)

[view on ChemRxiv](#) • [download file](#)

Photocatalytic Deoxygenation of N–O bonds with Rhenium Complexes: from the Reduction of Nitrous Oxide to Pyridine N-Oxides

Mariane Kjellberg, Alexia Ohleier, Pierre Thuéry, Emmanuel Nicolas, Lucile Anthore-Dalion,* and Thibault Cantat*
Université Paris-Saclay, CEA, CNRS, NIMBE, 91191 Gif-sur-Yvette CEDEX, FRANCE

Abstract

The accumulation of nitrogen oxides in the environment calls for new pathways to interconvert the various oxidation states of nitrogen, and especially their reduction. The large spectrum of reduction potentials covered by nitrogen oxides makes it however difficult to find general systems capable of efficiently reducing various N-oxides. Here photocatalysis unlocks high energy species able to both circumvent the inherent low reactivity of the greenhouse gas and oxidant N₂O ($E^\circ(\text{N}_2\text{O}/\text{N}_2) = +1.77$ V vs. SHE), and reduce pyridine N-oxides ($E_{1/2}(\text{pyridine } N\text{-oxide/pyridine}) = -1.04$ V vs. SHE). The rhenium complex [Re(4,4'-tBu-bpy)(CO)₃Cl] proved to be efficient to perform both reactions under ambient conditions, enabling the deoxygenation of N₂O as well as synthetically relevant and functionalized pyridine N-oxides.

Introduction

The modern development of intensive soil exploitation and – corollary – the massive production of nitrogen-based fertilizers from atmospheric N₂ has enabled to feed an ever-growing population.¹ Collateral damages however include increased production and accumulation of noxious nitrogen oxide wastes such as nitrates NO₃⁻, nitrites NO₂⁻ or nitrous oxide N₂O, their reduction back to N₂ being mostly ensured by the natural nitrogen cycle.^{2,3} As defined by environmental scientists, planetary boundaries for the biogeochemical nitrogen cycle have indeed already been crossed, the current nitrogen anthropogenic fixation representing more than twice the estimated boundary (150 Tg N/year vs. 62 Tg N/year).⁴⁻⁶ Since breaking the highly stable N₂ bond via the Haber-Bosch process consumes yearly 2% of the energy worldwide, leakage of nitrogen oxides in the environment represents as well a loss of energy.^{7,8} In the search for a more sustainable economy, there is hence a need of new pathways able to perform efficient interconversion between oxidation states of nitrogen, and especially reduction of nitrogen oxides to less oxidized molecules.⁹

Chemically speaking, this raises the issue of deoxygenating the N–O bond of both inorganic and organic N-oxides. With the aim to explore new pathways, we decided to harness the potential of homogeneous photoredox catalysis, which has already proven its utility in the deoxygenation of C–O bonds of C₁-molecules, such as CO₂.^{10,11} In contrast to their C₁-carbon counterparts,¹² nitrogen oxides cover a larger spectrum of reduction potentials (over 2.8 V vs. 0.4 V for CO₂) thus raising the level of difficulty to find general photocatalysts (Figure 1a).¹³

A simple model that can be used to showcase this deoxygenation is the ozone-depleting nitrous oxide N₂O, since it leads directly to N₂. Although N₂O is a strong oxidant ($E^\circ(\text{N}_2\text{O}/\text{N}_2) = +1.77$ V vs. SHE),¹³ homogeneous deoxygenation reactions are scarcely reported, for it is highly inert and a poorly coordinating molecule.^{14,15} Among the few thermocatalytic deoxygenating methods, the group

of Milstein disclosed the hydrogenation of N₂O to N₂ and H₂O catalyzed by a PNP pincer ruthenium complex at 65 °C, under a total pressure of 7 bar (Figure 1b).¹⁶ More recently, our laboratory proposed the deoxygenation of N₂O using disilanes and a catalytic amount of fluoride source under ambient conditions (Figure 1b).¹⁷ To the best of our knowledge, only heterogeneous photodeoxygenation of N₂O has been so far reported.¹⁸

At the opposite end of the redox scale, pyridine N-oxides have, in contrast, considerably lower reduction potentials ($E_{1/2}(\text{pyridine } N\text{-oxide (1a)/pyridine (2a)}) = -1.04$ V vs. SHE, Figure 1b) and they represent a much greater challenge.¹⁹ These compounds are useful intermediates in the synthesis of N-heteroaromatic-containing pharmaceutical or agrochemical products, where N-oxides are used for instance as directing groups for C–H bond functionalization.²⁰ In that context, there is a need for mild methods to post-reduce the N-oxide group and afford the N-heterocycle. The main reported methods involve sacrificial oxophilic reagents or high energy reductant based on phosphines,²¹ silane²² or borane²³ derivatives, with thermochemical or (photo)electrochemical activation.²⁴⁻²⁷ Nevertheless, all these methods imply the use of either heating systems or high energy reductants (with $E^\circ < 0$ V), leading to a loss of energy. There is moreover no report of systems capable of addressing the wide range of potentials (> 2.5 V) required to reduce both nitrous oxide and pyridine N-oxides.

Nevertheless, all these methods imply the use of either heating systems or high energy reductants (with $E^\circ < 0$ V), leading to a loss of energy. There is moreover no report of systems capable of addressing the wide range of potentials (> 2.5 V) required to reduce both nitrous oxide and pyridine N-oxides.

Herein, we disclose that a versatile photocatalytic system based on [Re(bpy)(CO)₃Cl]-type complexes²⁸ is able to efficiently deoxygenate both N₂O and pyridine N-oxides under ambient conditions (20 °C, 1 bar, Figure 1c).

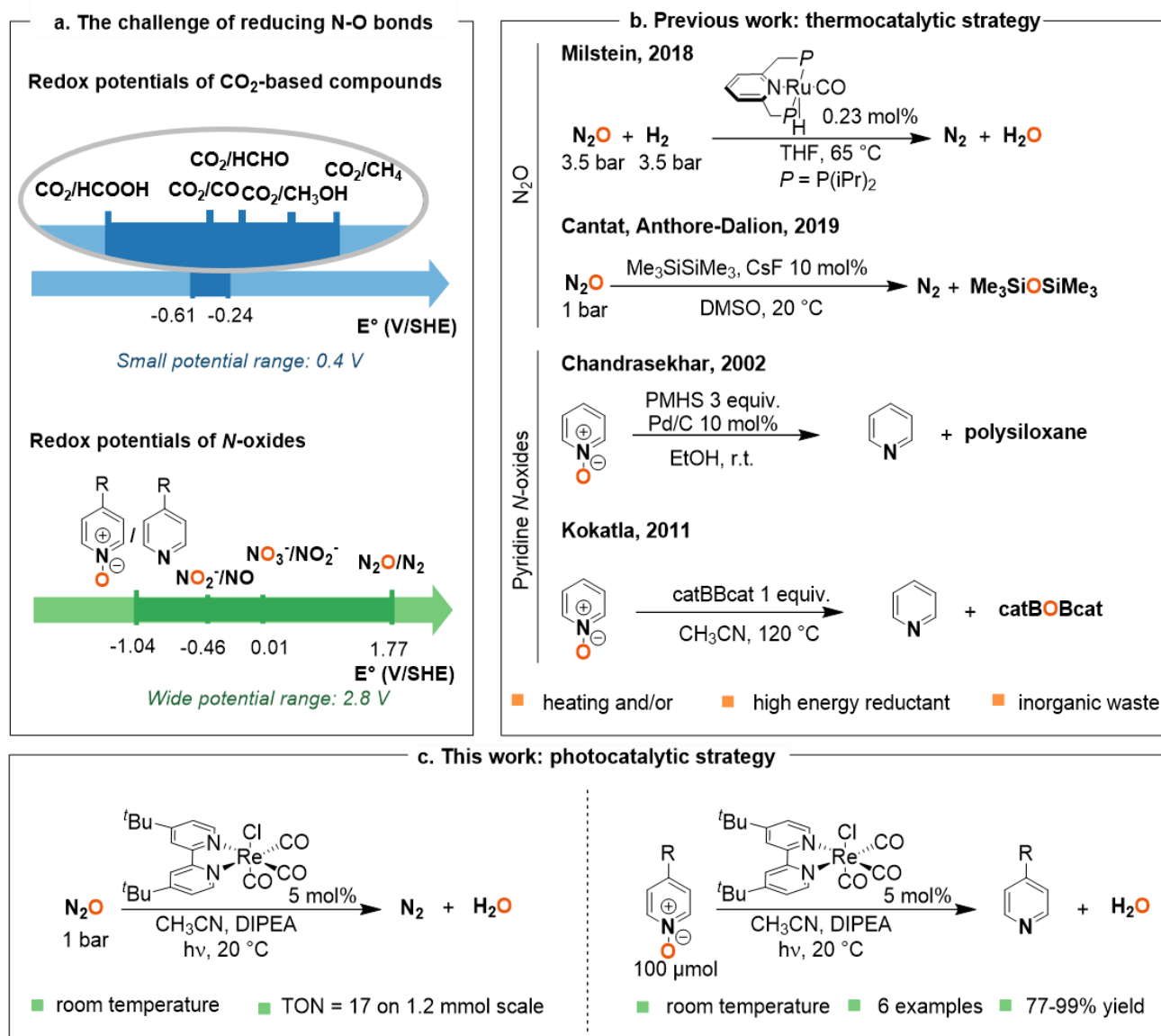


Figure 1. Development of a photocatalytic pathway to deoxygenate N–O bonds. **a**, Range of potentials involved for the reduction of C–O and N–O bonds. **b**, Existing strategies for N–O bond deoxygenation. **c**, Proposed strategy for the deoxygenation of N₂O and pyridine N-oxides. DIPEA, diisopropylethylamine.

Results and discussion

Design of the system for the photodeoxygenation of N₂O.

The potential of [Re(bpy)(CO)₃Cl] (**Re-1**) to photocatalyze the conversion of N₂O to N₂ was tested, using **Re-1** (5 mol%) as catalyst in acetonitrile in the presence of triethanolamine (TEOA) and 1 bar of N₂O. After 2 h of irradiation with white LEDs at 20 °C, N₂ was formed to our delight in 66% yield according to GC analysis of the gaseous fraction. This result represents the first homogeneous photocatalytic deoxygenation of N₂O to N₂ (Table 1, entry 1).

In the absence of **Re-1**, no conversion of N₂O was observed: cleavage of the N–O bond does not occur spontaneously under irradiation (Table 1, entry 2). Other blank experiments confirmed that no N₂ is formed in the absence of light, N₂O, or electron donor (Table 1, entries 3–5).

Interestingly, the reaction performed without N₂O afforded H₂ as sole product, as a result from TEOA decomposition in the

presence of the catalyst under irradiation (Table 1, entry 4). The detection of traces of H₂ at the end of the reaction (1.5% of the gaseous phase, Table 1, entry 1) was thus ascribed to the use of TEOA. Sacrificial amines in photocatalysis are indeed known to supply the catalytic cycle not only with electrons but also protons, which can in turn be reduced by the photocatalyst to H₂.²⁹ This prompted us to investigate the influence of the sacrificial electron donor on the outcome of N₂O photocatalytic reduction. Another tertiary amine, triethylamine (TEA), was used, inducing a drop of the N₂O conversion, the gaseous fraction of N₂ after 2 h decreasing from 66% down to 36% without suppressing the generation of H₂ (Table 1, entry 6). Since H₂ was likely produced through reduction of the protons located α to the nitrogen atom,³⁰ choice was made to use a bulkier tertiary amine, diisopropylethylamine (DIPEA, Hünig's base). When DIPEA was used as electron donor, H₂ could not be detected in GC after 2 hours of irradiation, and the N₂ yield increased up to 76% (Table

1, entry 7). We therefore selected DIPEA as the sacrificial electron donor for the rest of our study.

Table 1: Photodeoxygenation of N_2O catalyzed by **Re-1** and control experiments.

Entry	Deviation from standard conditions ^[a]	% H_2 ^[b]	% N_2 ^[b]	% N_2O ^[b]
1	None	1.5	66	32
2	No photocatalyst	0	2	98
3	No light	0	4	96
4	No N_2O ^[c]	91	9	0
5	No TEOA	0	8	92
6	TEA instead of TEOA	0.2	36	63
7	DIPEA instead of TEOA	0	76	24

[a] Standard reaction conditions: N_2O (1 bar, 100 μ mol), **Re-1** (5 μ mol, 5 mol%), CD_3CN (0.5 mL), donor (0.1 mL), 2 h, 20 °C. [b] Determined by GC analysis of the gaseous phase. Percentages correspond to the fraction of named gas in the overall analyzed gaseous phase (corrected with response factors). [c] Under argon (1 bar). TEOA: triethanolamine; TEA: trimethylamine; DIPEA: diisopropylethylamine.

Catalyst optimization. When the reaction was scaled up from 0.1 to 1.2 mmol N_2O , the yield with **Re-1** as catalyst dropped to 50%, affording a TON of 10 and a TOF₀ of 1.9 h⁻¹ (Table 2, entry 1). GC-monitoring showed no evolution after 22 h of reaction, indicating potential deactivation of the catalyst. We hence explored the effects of substitution on the bipyridine ligand. We synthesized a series of [Re(bpy)(CO)₃Cl]-type catalysts with bipyridines substituted either on the 4,4' or the 6,6'-position, and we studied their ability to photocatalyze the deoxygenation of N_2O (Figure 2a).

Complexes **Re-2**³¹ and **Re-3**³² possessing bipyridines substituted in the 4,4'-position with methyl or *t*-butyl groups, respectively, were also active in the deoxygenation of N_2O , and led to higher yields in N_2 than unsubstituted **Re-1**, 70% and 86% respectively, corresponding to TONs of 14 and 17. They also showed higher activity than **Re-1**: TOF₀ reached 3.7 h⁻¹ and 4.3 h⁻¹ for **Re-2** and **Re-3** respectively vs. 0.7 h⁻¹ for **Re-1** (Table 2, entries 1-3). On the other hand, **Re-4**³¹ and the novel **Re-5** complex, featuring methyl and bulky mesityl substituents in the 6 and 6' positions of bipyridines, were less efficient on a 24 h timescale, leading to moderate

yields in N_2 of 55% and 61% respectively (Table 2, entries 4 and 5). This behavior is also present in their initial activities: lower TOF₀ (2.7 and 1.1 h⁻¹ for **Re-4** and **Re-5** respectively) were measured compared to **Re-2** and **Re-3**.

A more precise monitoring of kinetic profiles for each catalyst was also performed (Figure 2b). The evolution of the N_2 yield over 60 h showed that **Re-1** deactivated after 22 h, sooner than all the other substituted catalysts, which accounts for the low yields obtained with **Re-1**. In contrast, **Re-2** and **Re-3**, presenting *para*-substituted bipyridines, showed both high catalytic activity and increased stability. This phenomenon has been studied in the case of CO₂ electroreduction by Kubiak et al.: they showed that substituting the bipyridine ligand in the 4,4'-positions provided sufficient steric hindrance to inhibit the dimerization of a Re(0) reactive intermediate to an inactive bimetallic complex.³³⁻³⁶ The stability increased with the steric bulk of the substituent. The same tendency is observed here in the case of the photoreduction of N_2O , and hints towards a similar mechanistic pathway. Complexes **Re-4** and **Re-5**, substituted in the *ortho* position, demonstrated an increased stability compared to **Re-1** but, interestingly enough, the increase in stability brought by substitution on the bipyridine did not come along with an increase in activity. These catalysts indeed required respectively 100 h and 150 h to yield 55% and 61% of N_2 . A structural explanation could arise from the steric strain between the substituents on the bipyridine and the equatorial carbonyls in **Re-4** and **Re-5**.

Rhenium photocatalysts of type [Re(bpy)(CO)₃Cl] are thus able to catalyze the deoxygenation of N_2O , suggesting that other N–O bonds could be deoxygenated under similar reaction conditions.

Table 2: Performances of the photocatalysts in the deoxygenation of N_2O

Entry	Catalyst	TOF ₀ (h ⁻¹)	% N_2 (TON)	Time (h)
1	Re-1	1.9	50 (10)	22
2	Re-2	3.7	70 (14)	50
3	Re-3	4.3	86 (17)	115
4	Re-4	2.7	55 (11)	100
5	Re-5	1.1	61 (12)	150

Reaction conditions: N_2O (1.0 bar, 1.2 mmol), catalyst (60 μ mol, 5 mol%), CH_3CN (7.2 mL), DIPEA (1.4 mL), 20 °C

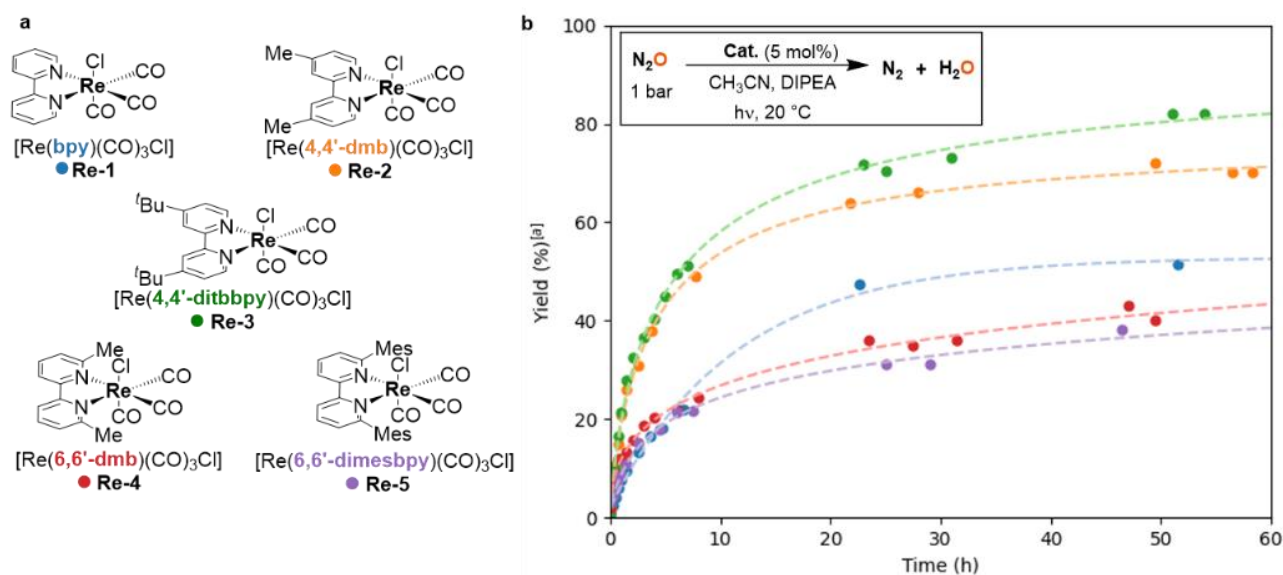


Figure 2. Photodeoxygenation of N_2O : screening of catalysts. *a*, Photocatalysts **Re-1–5** used in the study. *b*, Kinetic profiles on 1.2 mmol scale. Reaction conditions: N_2O (1.0 bar, 1.2 mmol), catalyst (5 mol%), CH_3CN (7.2 mL), DIPEA (1.4 mL), 20 °C

Photodeoxygenation of pyridine N-oxides. Encouraged by the success of N_2O deoxygenation, we considered the possibility of applying this methodology to the deoxygenation of more challenging N–O bonds across the scale of redox potentials, namely of pyridine *N*-oxides ($E_{1/2}(\text{pyridine } N\text{-oxide (1a)}/\text{pyridine (2a)}) = -1.04$ V vs. SHE). Although they present lower reduction potentials compared to that of N_2O ($E^\circ(N_2O/N_2) = +1.77$ V vs. SHE), we envisaged that rhenium-based catalysts should be able to deoxygenate as well their N–O bond ($E^\circ(\text{Re-3}/\text{Re-3}^+) = -1.21$ V vs. SHE).³³ The reaction was monitored by NMR using rhenium-based **Re-1–5** photocatalysts. To our delight, a first attempt using the *t*Bu-substituted catalyst **Re-3** under the reaction conditions developed for N_2O enabled to deoxygenate pyridine *N*-oxide (**1a**) to pyridine (**2a**) in 82% yield after 34 h (Table 3, entry 1). The blank experiments confirmed that all components (light, photocatalyst, electron donor) were necessary to perform the reduction (see Supplementary Table S1). Remarkably, the other catalysts also afforded full conversion of compound **1a**, albeit with longer reaction times (44–87 h), leading to pyridine (**2a**) in 85–99% yield (Table 3, entries 2–5). This stands in contrast with our observations with N_2O : here the yields showed steady increase until full conversion with all catalysts. Two explanations may arise for this phenomenon: either the pyridine produced during the reaction delays catalyst deactivation through the stabilization of reactive intermediates,³⁷ or the higher oxidative character of N_2O has a detrimental effect on the catalyst stability. This effect was particularly beneficial in the case of the 6,6'-dimethylbipyridine rhenium complex **Re-4**, which led only to 55% yield of N_2 after 100 h and gave full conversion of pyridine *N*-oxide (**1a**) within 55 h. Again, 4,4'-substituted catalysts **Re-2** and **Re-3** displayed higher catalytic activity ($TOF_0 = 11$ and 16 h⁻¹) than unsubstituted **Re-1** and 6,6'-

substituted **Re-4** and **Re-5** ($TOF_0 = 5.5$, 7.5 and 2.6 h⁻¹, respectively), suggesting similar mechanistic patterns for the deoxygenation of both N_2O and pyridine *N*-oxide (**1a**) (Table 3). To study the effect of irradiation, a light on/light off experiment was also performed (Figure 3a).³⁸ The substrate was only converted when the system was exposed to light, and the reaction stopped once the system was in the dark. Continuous irradiation is thus required to perform the reaction. From a kinetic standpoint, the possible improvement of catalytic performances as pyridine was released was particularly noticeable in the case of 6,6'-substituted catalysts **Re-4** and **Re-5**. If their initial catalytic activities were low ($TOF_0 = 7.5$ and 2.6 h⁻¹), they showed steady catalytic activity past 2 hours of irradiation, while the conversion rates for the other catalysts were gently decreasing (Figure 3b). This resulted in **Re-4** and **Re-5** reaching full conversion before **Re-1** and **Re-2**.

Table 3: Photocatalytic deoxygenation of pyridine *N*-oxide with different photocatalysts

Entry	Cat.	TOF_0 (h ⁻¹)	Yield (%)	Time to full conversion (h)
1	Re-3	16	82	34
2	Re-1	5.5	99	63
3	Re-2	11	85	87
4	Re-4	7.5	96	55
5	Re-5	2.6	87	44

Reaction conditions: pyridine *N*-oxide (100 μmol), catalyst (5 μmol, 5 mol%), CD_3CN (0.5 mL), DIPEA (0.1 mL), 20 °C

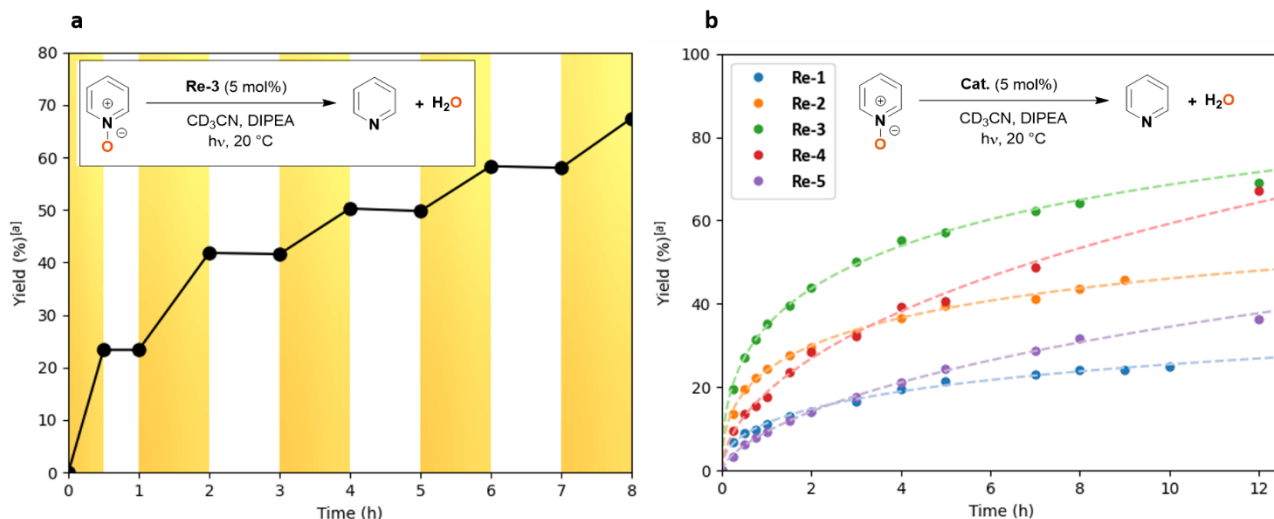


Figure 3. Photoreduction of pyridine *N*-oxide. **a**, Light and dark experiment with **Re-3**. Yellow: light on; white: light off. **b**, Kinetic profiles of pyridine *N*-oxide photoreduction with different catalysts. Reaction conditions: pyridine *N*-oxide (100 μmol), catalyst (5 μmol , 5 mol%), CD_3CN (0.5 mL), DIPEA (0.1 mL), 20 $^\circ\text{C}$. [a] Determined by ^1H NMR analysis of the crude reaction mixture.

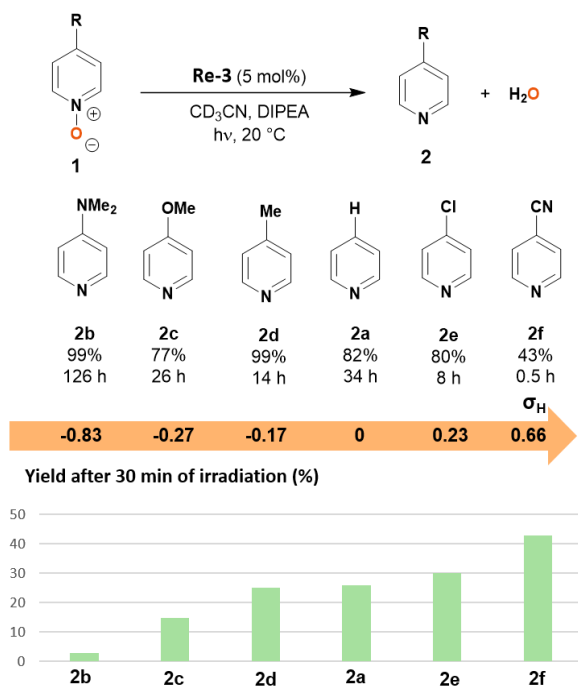


Figure 4. Photocatalytic reduction of *para*-substituted pyridine *N*-oxides. **a**, Scope of substrates (yield, time of irradiation until maximum yield). Corresponding Hammett constants of the substituents. Reaction conditions: pyridine *N*-oxide (100 μmol), **Re-3** (5 μmol , 5 mol%), CD_3CN (0.5 mL), DIPEA (0.1 mL), 20 $^\circ\text{C}$. Yields were determined by ^1H NMR analysis of the crude reaction mixture. **b**, Yields of the photocatalytic deoxygenation of *para*-substituted pyridine *N*-oxides after 30 minutes of irradiation.

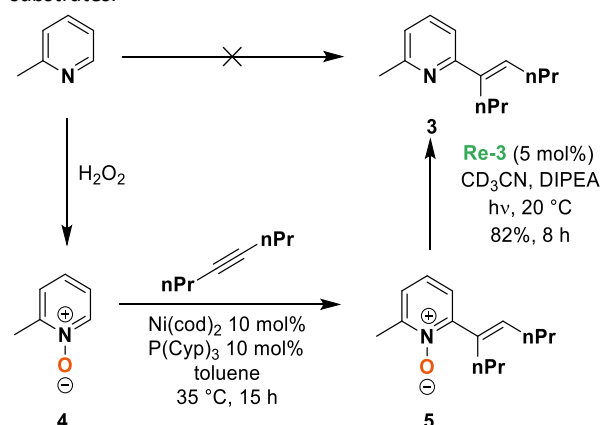
Several *para*-substituted pyridine *N*-oxides **1b-f** could be deoxygenated in 77-99% yield using photocatalyst **Re-3** (Figure 4). The electronic parameters of the substituents affected the initial reaction rate: the yields after 30 min of irradiation evolved in line with the electron-withdrawing ability of the substituents as given by their Hammett sigma constants (Figure 4b).³⁹ Indeed, compounds

bearing electron-donating substituents were only poorly converted after 30 min.: **1b-d** bearing dimethylamino, methoxy or methyl groups ($\sigma_{\text{H}} = -0.83$, -0.27 and -0.17 respectively) reached only 3 to 25% yield, while **1a**, **1e** and **1f**, bearing $-\text{H}$, chloro or cyano groups ($\sigma_{\text{H}} = 0$, 0.23 and 0.66 respectively) yielded after 30 min. 26, 30 and 43% of the corresponding pyridines, respectively. This was also reflected in the time to reach full conversion: pyridine *N*-oxides **1b-d** bearing electron-donating substituents ($-\text{NMe}_2$, $-\text{OMe}$, $-\text{Me}$) in the *para* position required longer reaction times (14-126 h) than **1e-f** with electron-withdrawing substituents (8 and 0.5 h respectively for the chloro and cyano derivatives). In particular the conversion of the nitrile derivative **1f** was extremely fast, maximal (43%) after only 30 min of irradiation. Further irradiation however led to over-reduction of **2f** to pyridine **2a** (for details see Supplementary Fig. S1).

This is the first photocatalytic system able to perform such a deoxygenation reaction without additional energy sources. In contrast, strong reductants based on Hantzsch esters or hydrazine were used by the groups of Konev and Wangelin²⁶ and Lee.²⁷

In order to demonstrate the selectivity of this reaction and its synthetic utility, we explored the deoxygenation of a more complex substrate, that is a 2,6-substituted pyridine *N*-oxide. Pyridine *N*-oxide indeed feature an enhanced reactivity compared to the reduced pyridine, enabling the functionalization of the 2,6-positions by C-H activation and, as an example, Hiyama et al. recently reported the synthesis of 2,6-substituted pyridine **3**, based on the oxidation of *o*-picoline to form the 2-methylpyridine *N*-oxide **4**.⁴⁰ A Ni-catalyzed coupling reaction leads to 2,6 substituted pyridine *N*-oxide **5**, whose deoxygenation presents multiple challenges that are chemoselectivity and steric hindrance. In their publication, the group of Hiyama used PCl_3 as a reducing agent to perform such a deoxygenation. We were very pleased to observe that using our system, **Re-3** catalyzed the

deoxygenation with 82 % yield after 8 h of irradiation (Scheme 1). This demonstrates the validity of such an approach for mild deprotection strategies, which may be extended to other substrates.



Scheme 1. 2-Methylpyridine functionalization via the N-oxide strategy

Conclusion

In summary, a new photochemical method has been developed to deoxygenate N–O bonds with radically different reduction potentials, over a 2.8 V window. [Re(4,4'-tBu-bpy)(CO)₃Cl] (**Re-3**) is indeed capable of reducing both N₂O under ambient conditions, and pyridine N-oxides **1** and **4** in good to excellent yields. Those results open new perspectives concerning the photocatalytic deoxygenation of nitrogen oxide-containing compounds. Further mechanistic studies on catalyst **Re-3** are underway in our laboratory. We believe that these will give new clues to understanding N–O bonds deoxygenation chemistry.

Acknowledgements

We thank the CEA, CNRS, ERC (Consolidator Grant n° 818260), and Institut de France for funding. M.K. was supported by a PhD fellowship from ADEME. We thank Thierry Bernard (CEA) for the help in conception and realization of the photochemistry reactor.

Data availability

Data relating to the characterization data of materials and products, general methods, optimization studies, experimental procedures, gas chromatography and NMR spectra are available in the Supplementary Information. Crystallographic data for compounds **Re-4** and **Re-5** are available free of charge from the Cambridge Crystallographic Data Centre (CCDC) under reference numbers 2056048 and 2056049, respectively.

References

- Mosier, A., Syers, J. K. & Freney, J. R. *Agriculture and the Nitrogen Cycle: Assessing the Impacts of Fertilizer Use on Food Production and the Environment*. (Island Press, 2013).
- Lehnert, N., Dong, H. T., Harland, J. B., Hunt, A. P. & White, C. J. Reversing nitrogen fixation. *Nat. Rev. Chem.* **2**, 278-289 (2018).

- Tian, H., Xu, R., Canadell, J. G., Thompson, R. L., Winiwarter, W., Suntharalingam, P., Davidson, E. A., Ciais, P., Jackson, R. B., Janssens-Maenhout, G., Prather, M. J., Regnier, P., Pan, N., Pan, S., Peters, G. P., Shi, H., Tubiello, F. N., Zaehle, S., Zhou, F., Arneeth, A., Battaglia, G., Berthet, S., Bopp, L., Bouwman, A. F., Buitenhuis, E. T., Chang, J., Chipperfield, M. P., Dangal, S. R. S., Dlugokencky, E., Elkins, J. W., Eyre, B. D., Fu, B., Hall, B., Ito, A., Joos, F., Krummel, P. B., Landolfi, A., Laruelle, G. G., Lauerwald, R., Li, W., Lienert, S., Maavara, T., MacLeod, M., Millet, D. B., Olin, S., Patra, P. K., Prinn, R. G., Raymond, P. A., Ruiz, D. J., van der Werf, G. R., Vuichard, N., Wang, J., Weiss, R. F., Wells, K. C., Wilson, C., Yang, J. & Yao, Y. A comprehensive quantification of global nitrous oxide sources and sinks. *Nature* **586**, 248-256 (2020).
- Rockström, J., Steffen, W., Noone, K., Persson, Å., Chapin, F. S., Lambin, E. F., Lenton, T. M., Scheffer, M., Folke, C., Schellnhuber, H. J., Nykvist, B., de Wit, C. A., Hughes, T., van der Leeuw, S., Rodhe, H., Sörlin, S., Snyder, P. K., Costanza, R., Svedin, U., Falkenmark, M., Karlberg, L., Corell, R. W., Fabry, V. J., Hansen, J., Walker, B., Liverman, D., Richardson, K., Crutzen, P. & Foley, J. A. A safe operating space for humanity. *Nature* **461**, 472-475 (2009).
- de Vries, W., Kros, J., Kroeze, C. & Seitzinger, S. P. Assessing planetary and regional nitrogen boundaries related to food security and adverse environmental impacts. *Curr. Opin. Sust.* **5**, 392-402 (2013).
- Steffen, W., Richardson, K., Rockström, J., Cornell, S. E., Fetzer, I., Bennett, E. M., Biggs, R., Carpenter, S. R., de Vries, W., de Wit, C. A., Folke, C., Gerten, D., Heinke, J., Mace, G. M., Persson, L. M., Ramanathan, V., Reyers, B. & Sörlin, S. Planetary boundaries: Guiding human development on a changing planet. *Science* **347**, 1259855 (2015).
- Chen, S., Perathoner, S., Ampelli, C. & Centi, G., Chapter 2 - Electrochemical Dinitrogen Activation: To Find a Sustainable Way to Produce Ammonia in *Stud. Surf. Sci. Catal.* Vol. 178 (eds Stefania Albonetti, Siglinda Perathoner, & Elsjé Alessandra Quadrelli) 31-46 (Elsevier, 2019).
- Elishav, O., Mosevitzky Lis, B., Miller, E. M., Arent, D. J., Valera-Medina, A., Grinberg Dana, A., Shter, G. E. & Grader, G. S. Progress and Prospective of Nitrogen-Based Alternative Fuels. *Chem. Rev.* **120**, 5352-5436 (2020).
- Chen, J. G., Crooks, R. M., Seefeldt, L. C., Bren, K. L., Bullock, R. M., Darensbourg, M. Y., Holland, P. L., Hoffman, B., Janik, M. J., Jones, A. K., Kanatzidis, M. G., King, P., Lancaster, K. M., Lymar, S. V., Pfromm, P., Schneider, W. F. & Schrock, R. R. Beyond fossil fuel-driven nitrogen transformations. *Science* **360**, eaar6611 (2018).
- Yamazaki, Y., Takeda, H. & Ishitani, O. Photocatalytic reduction of CO₂ using metal complexes. *J. Photochem. Photobiol. C: Photochem. Rev.* **25**, 106-137 (2015).
- Kuramochi, Y., Ishitani, O. & Ishida, H. Reaction mechanisms of catalytic photochemical CO₂

- reduction using Re(I) and Ru(II) complexes. *Coord. Chem. Rev.* **373**, 333-356 (2018).
- 12 Chauvier, C. & Cantat, T. A Viewpoint on Chemical Reductions of Carbon–Oxygen Bonds in Renewable Feedstocks Including CO₂ and Biomass. *ACS Catal.* **7**, 2107-2115 (2017).
- 13 Lide, D. R. *CRC handbook of chemistry and physics*. Vol. 85 (CRC press, 2004).
- 14 Parmon, V. N., Panov, G. I., Uriarte, A. & Noskov, A. S. Nitrous oxide in oxidation chemistry and catalysis: application and production. *Catal. Today* **100**, 115-131 (2005).
- 15 Severin, K. Synthetic chemistry with nitrous oxide. *Chem. Soc. Rev.* **44**, 6375-6386 (2015).
- 16 Zeng, R., Feller, M., Ben-David, Y. & Milstein, D. Hydrogenation and Hydrosilylation of Nitrous Oxide Homogeneously Catalyzed by a Metal Complex. *Journal of the American Chemical Society* **139**, 5720-5723 (2017).
- 17 Anthore-Dalio, L., Nicolas, E. & Cantat, T. Catalytic Metal-Free Deoxygenation of Nitrous Oxide with Disilanes. *ACS Catal.* **9**, 11563-11567 (2019).
- 18 Ming, T., de Richter, R., Shen, S. & Caillol, S. Fighting global warming by greenhouse gas removal: destroying atmospheric nitrous oxide thanks to synergies between two breakthrough technologies. *Environ. Sci. Pollut. Res.* **23**, 6119-6138 (2016).
- 19 Kubota, T. & Miyazaki, H. The Effect of Substituents on the Half-Wave Potential of the Polarographic Reduction of Pyridine N-Oxide Derivatives. *Bull. Chem. Soc. Jpn.* **39**, 2057-2062 (1966).
- 20 Wang, Y. & Zhang, L. Recent Developments in the Chemistry of Heteroaromatic N-Oxides. *Synthesis* **47**, 289-305 (2015).
- 21 Howard, E. & Olszewski, W. F. The Reaction of Triphenylphosphine with Some Aromatic Amine Oxides. *Journal of the American Chemical Society* **81**, 1483-1484 (1959).
- 22 Chandrasekhar, S., Reddy, C. R., Rao, R. J. & Rao, J. M. Efficient and Chemoselective Deoxygenation of Amine N-Oxides Using Polymethylhydrosiloxane. *Synlett* **2002**, 0349-0351 (2002).
- 23 Kokatla, H. P., Thomson, P. F., Bae, S., Doddi, V. R. & Lakshman, M. K. Reduction of Amine N-Oxides by Diboron Reagents. *J. Org. Chem.* **76**, 7842-7848 (2011).
- 24 Xu, P. & Xu, H. C. Electrochemical Deoxygenation of N-Heteroaromatic N-Oxides. *Synlett* **30**, 1219-1221 (2019).
- 25 Fukazawa, Y., Rubtsov, A. E. & Malkov, A. V. A Mild Method for Electrochemical Reduction of Heterocyclic N-Oxides. *Eur. J. Org. Chem.* **2020**, 3317-3319 (2020).
- 26 Konev, M. O., Cardinale, L. & Jacobi von Wangelin, A. Catalyst-Free N-Deoxygenation by Photoexcitation of Hantzsch Ester. *Org. Lett.* **22**, 1316-1320 (2020).
- 27 Kim, K. D. & Lee, J. H. Visible-Light Photocatalyzed Deoxygenation of N-Heterocyclic N-Oxides. *Org. Lett.* **20**, 7712-7716 (2018).
- 28 Hawecker, J., Lehn, J.-M. & Ziessel, R. Efficient photochemical reduction of CO₂ to CO by visible light irradiation of systems containing Re(bipy)(CO)₃X or Ru(bipy)₃²⁺-Co²⁺ combinations as homogeneous catalysts. *J. Chem. Soc., Chem. Commun.*, 536-538 (1983).
- 29 Hu, J., Wang, J., Nguyen, T. H. & Zheng, N. The chemistry of amine radical cations produced by visible light photoredox catalysis. *Beilstein Journal of Organic Chemistry* **9**, 1977-2001 (2013).
- 30 Meister, S., Reithmeier, R. O., Tschurl, M., Heiz, U. & Rieger, B. Unraveling Side Reactions in the Photocatalytic Reduction of CO₂: Evidence for Light-Induced Deactivation Processes in Homogeneous Photocatalysis. *ChemCatChem* **7**, 690-697 (2015).
- 31 Kalyanasundaram, K. Luminescence and redox reactions of the metal-to-ligand charge-transfer excited state of tricarbonylchloro-(polypyridyl)rhenium(I) complexes. *J. Chem. Soc., Faraday Trans. 2* **82**, 2401-2415 (1986).
- 32 Yam, V. W.-W., Lau, V. C.-Y. & Cheung, K.-K. Synthesis and Photophysics of Luminescent Rhenium(I) Acetylides-Precursors for Organometallic Rigid-Rod Materials. X-ray Crystal Structures of [Re(tBu₂bpy)(CO)₃(tBuCC)] and [Re(tBu₂bpy)(CO)₃Cl]. *Organometallics* **14**, 2749-2753 (1995).
- 33 Smieja, J. M. & Kubiak, C. P. Re(bipy-tBu)(CO)₃Cl-improved Catalytic Activity for Reduction of Carbon Dioxide: IR-Spectroelectrochemical and Mechanistic Studies. *Inorg. Chem.* **49**, 9283-9289 (2010).
- 34 Smieja, J. M., Benson, E. E., Kumar, B., Grice, K. A., Seu, C. S., Miller, A. J. M., Mayer, J. M. & Kubiak, C. P. Kinetic and structural studies, origins of selectivity, and interfacial charge transfer in the artificial photosynthesis of CO. *PNAS* **109**, 15646 (2012).
- 35 Benson, E. E., Kubiak, C. P., Sathrum, A. J. & Smieja, J. M. Electrocatalytic and homogeneous approaches to conversion of CO₂ to liquid fuels. *Chem. Soc. Rev.* **38**, 89-99 (2009).
- 36 Benson, E. E. & Kubiak, C. P. Structural investigations into the deactivation pathway of the CO₂ reduction electrocatalyst Re(bpy)(CO)₃Cl. *Chem. Commun.* **48**, 7374-7376 (2012).
- 37 Hawecker, J., Lehn, J.-M. & Ziessel, R. Photochemical and Electrochemical Reduction of Carbon Dioxide to Carbon Monoxide Mediated by (2,2'-Bipyridine)tricarbonylchlororhenium(I) and Related Complexes as Homogeneous Catalysts. *Helv. Chim. Acta* **69**, 1990-2012 (1986).
- 38 Buzzetti, L., Crisenza, G. E. M. & Melchiorre, P. Mechanistic Studies in Photocatalysis. *Angew. Chem. Int. Ed.* **58**, 3730-3747 (2019).
- 39 Hammett, L. P. The Effect of Structure upon the Reactions of Organic Compounds. Benzene Derivatives. *Journal of the American Chemical Society* **59**, 96-103 (1937).
- 40 Kanyiva, K. S., Nakao, Y. & Hiyama, T. Nickel-Catalyzed Addition of Pyridine-N-oxides across Alkynes. *Angew. Chem. Int. Ed.* **46**, 8872-8874 (2007).

text-preprint.pdf (1.17 MiB)

[view on ChemRxiv](#) • [download file](#)

Supporting Information for
Photocatalytic Deoxygenation of N–O bonds with Rhenium
Complexes: from the Reduction of Nitrous Oxide to Pyridine N-
Oxides

Marianne Kjellberg, Alexia Ohleier, Pierre Thuéry, Emmanuel Nicolas, Lucile
Anthore-Dalion,* and Thibault Cantat*

NIMBE, CEA, CNRS, Université Paris-Saclay, CEA Saclay, 91191 Gif sur Yvette Cedex
Tel: +33 1 69 08 43 38 ; Fax: +33 1 69 08 66 40
E-mail: lucile.anthore-dalion@cea.fr, thibault.cantat@cea.fr

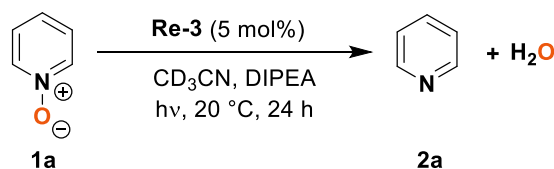
1	SUPPLEMENTARY DATA	S3
1.1	CONTROL EXPERIMENTS FOR THE PHOTOCATALYTIC REDUCTION OF PYRIDINE N-OXIDE 1A	S3
1.2	PHOTOCATALYTIC REDUCTION OF 4-CYANOPYRIDINE N-OXIDE 1F	S3
2	EXPERIMENTAL DETAILS	S5
2.1	MATERIAL AND METHODS	S5
2.1.1	<i>General</i>	S5
2.1.2	<i>Experimental setup for irradiation</i>	S5
2.2	SYNTHETIC PROCEDURES FOR CATALYSTS	S6
2.2.1	<i>Synthesis of [Re(6,6'-dmb)(CO)₃Cl] Re-4</i>	S6
2.2.2	<i>Synthesis of [Re(6,6'-mesbpy)(CO)₃Cl] Re-5</i>	S7
2.3	PHOTOCATALYTIC PROCEDURES	S9
2.3.1	<i>Photocatalytic reduction of N₂O on NMR scale</i>	S9
2.3.2	<i>Photocatalytic reduction of N₂O on a 1.2 mmol scale</i>	S9
2.3.3	<i>Photocatalytic reduction of pyridine N-oxides</i>	S10
3	GC ANALYSES	S12
3.1	GC CONDITIONS	S12

3.2	GC CALIBRATION	S12
3.3	ANALYSIS OF THE GASEOUS FRACTION FROM A J-YOUNG NMR TUBE	S13
4	ANALYSIS DATA	S15
4.1	LUMINESCENCE QUENCHING EXPERIMENTS	S15
4.2	CRYSTALLOGRAPHY	S16
4.3	COPIES OF NMR SPECTRA	S18
4.3.1	Re-4	S18
4.3.2	Re-5	S19
4.4	COPIES OF GC TRACES	S20
4.4.1	<i>Representative GC traces for the photocatalyzed reduction of N₂O by Re-3</i>	S20
4.4.2	<i>GC trace for the reduction of N₂O catalyzed by Re-1 in presence of TEOA</i>	S21
4.4.3	<i>GC traces for the control experiments for the photoreduction of N₂O with Re-1 (see Table 1)</i>	S22
4.5	COPIES OF UV-VIS SPECTRA.....	S24
4.5.1	<i>Absorption spectrum of Re-4</i>	S24
4.5.2	<i>Absorption spectrum of Re-5</i>	S25
5	REFERENCES.....	S26

1 Supplementary Data

1.1 Control experiments for the photocatalytic reduction of pyridine N-oxide **1a**

Table S1: Photocatalytic reduction of pyridine N-oxide **6a** and control experiments



Entry	Deviation from standard conditions ^[a]	Conversion of 1a (%) ^[b]	Yield of 2a (%) ^[b]
1	None	100	78
2	No light	0	0
3	No photocatalyst	0	0
4	No pyridine N-oxide	0	0
5	No DIPEA	0	0

[a] Standard reaction conditions: **6a** (100 μmol), **Re-3** (5 μmol , 5 mol%), CD_3CN (0.5 mL), DIPEA (0.1 mL), 20 °C, 24 h of irradiation.

[b] Conversions and yields measured by ^1H NMR analysis of the crude reaction mixture (internal standard: mesitylene).

1.2 Photocatalytic reduction of 4-cyanopyridine N-oxide **1f**

In the case of the photocatalytic reduction of **1f**, the conversion to **2f** was maximal (77%) after 30 minutes of irradiation. Further irradiation of the same NMR tube afforded pyridine **2a** in 100% conversion after 8 hours (Figure S1). The decyanation of **2f** to **2a** by irradiation of $[\text{Re}(\text{bpy})(\text{CO})_3(\mathbf{2f})]^+$ in DMF:TEOA was reported by the group of Ishitani, affording $[\text{Re}(\text{bpy})(\text{CO})_3(\text{CN})]$ and free pyridine **2a**.¹ Thus, the conversion of **2f** to **2a** observed here is proposed to occur *via* the formation of intermediate $[\text{Re}(\text{bpy})(\text{CO})_3(\mathbf{2f})]^+$.

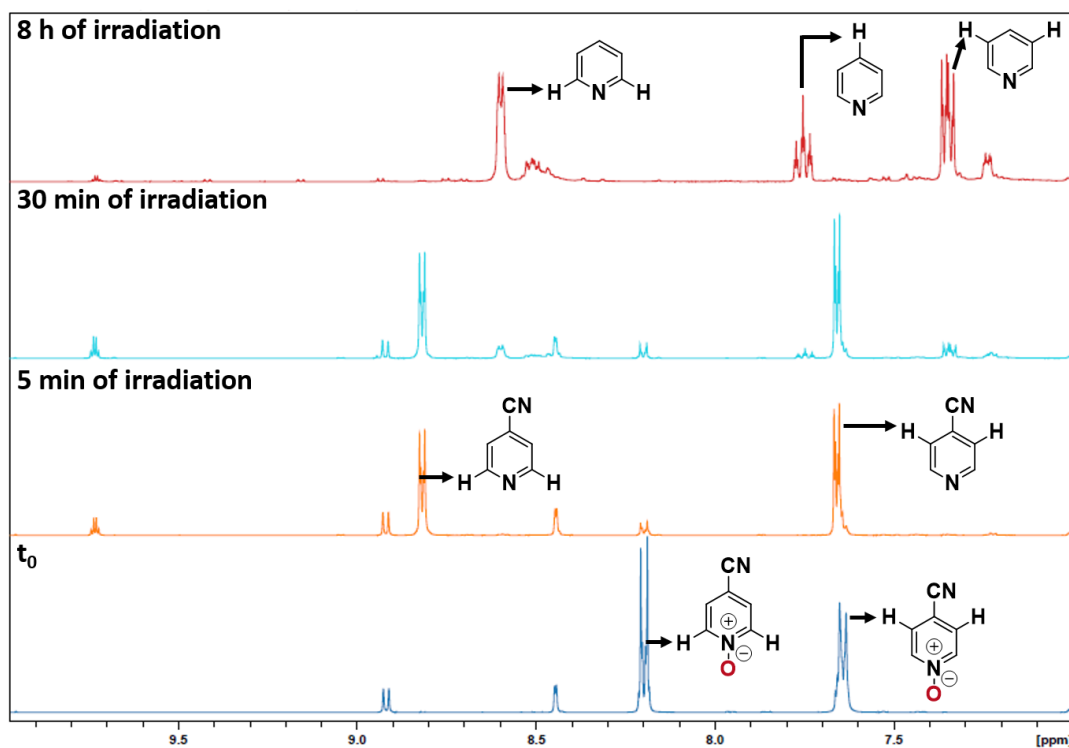
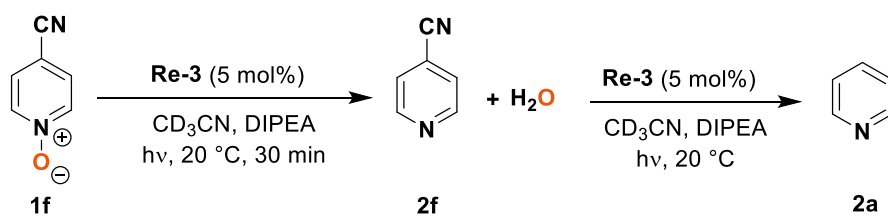


Figure S1: Photocatalytic reduction of 4-cyanopyridine N-oxide **1f** with **Re-3**: evolution of the reaction mixture (¹H NMR, aromatic region).

2 Experimental Details

2.1 Material and methods

2.1.1 General

All reactions and manipulations were performed at 20 °C in a recirculating mBraun LabMaster DP inert atmosphere (Ar) drybox and/or using Schlenk lines. Glassware was dried overnight at 120 °C. Unless otherwise stated, all the reagents were purchased from commercial suppliers (Aldrich, Acros, Alfa Aesar, TCI). Nitrous oxide was purchased from Messer (purity \geq 99,998%). Non deuterated solvents were thoroughly dried and distilled by standard methods prior to use. Deuterated solvents were dried on molecular sieves (4 Å; Aldrich) before use. ^1H and ^{13}C NMR spectra were recorded on a Bruker Advance Neo spectrometer operating at 400 MHz for ^1H . Chemical shifts for ^1H and $^{13}\text{C}\{^1\text{H}\}$ NMR spectra were referenced to solvent impurities. Coupling constants J are given in Hz. The following abbreviations are used: s, singlet; d, doublet; t, triplet; m, multiplet. Gas chromatography data were collected on a Shimadzu GC-2010 Plus. UV-visible spectra were recorded on a PerkinElmer Lambda 900 spectrometer.

2.1.2 Experimental setup for irradiation

A custom-made irradiation setup was used for all photocatalytic experiments. It is constituted of a hexagonal aluminum chassis with 6 regularly disposed holes, one on each side. A Light Emitting Diode (cool white LED, GU5.3 / MR16 12V 8W SMD 80°, 6000-8000 K) is built into each hole. On top, the apparatus displays 6 equivalent positions that can host NMR tubes for reproducible irradiations, and one hole in the middle used for scale-up experiments (Figure S2, right). A cooling fan under the reactor enables to evacuate the heat produced by the absorbing solution and/or by exothermic reactions. The whole apparatus is supported by a magnetic stirrer; stirring enables to maximize the absorption of photons by the solution. In our experiments, stirring was performed at 300 rpm.

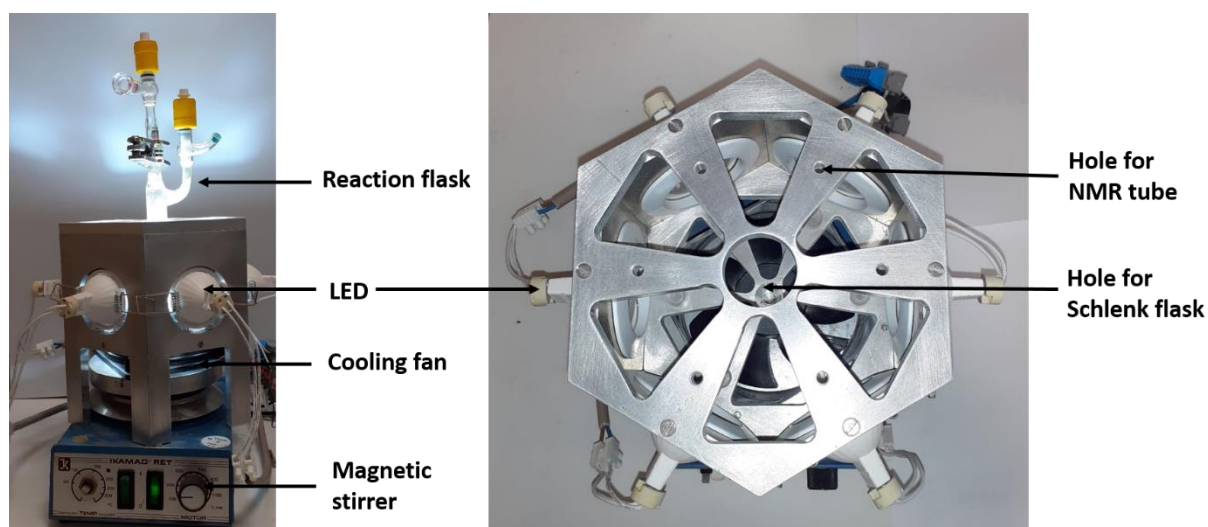
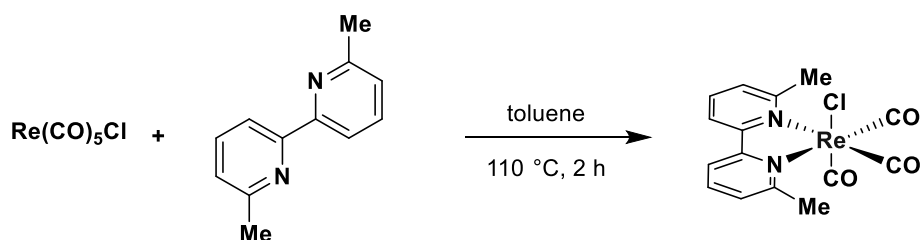


Figure S2: Sideview (left) and topview (right) of the setup used for irradiation.

2.2 Synthetic procedures for catalysts

Complexes **Re-1** to **Re-3** were prepared according to reported procedures.² The NMR data are in agreement with those reported in the literature.³ Complexes **Re-4** and **Re-5** were synthesized using the same methodology.

2.2.1 Synthesis of [Re(6,6'-dmb)(CO)₃Cl] **Re-4**



Scheme S1: Synthetic pathway towards [Re(6,6'-dmb)(CO)₃Cl] **Re-4**.

In a glovebox, a 50 mL round-bottomed flask equipped with a stirring bar and a *J-Young* valve was charged with 6,6'-dimethylbipyridine (88 mg, 478 μ mol, 1 equiv.), [Re(CO)₅Cl] (173 mg, 478 μ mol, 1 equiv.), and 15 mL of anhydrous toluene. The flask was sealed, brought out of the glovebox, and immersed in an oil bath at 110 °C. After 2 hours, the resulting yellow solution was cooled down to room temperature and the solvent was removed *in vacuo* to afford a crude yellow solid. The latter was suspended in pentane and centrifuged three times for 10 min. The solid was dried under vacuum overnight to give [Re(6,6'-dimethylbipyridine)(CO)₃Cl] **Re-4** (170 mg, 73%) as a yellow powder. Single crystals suitable for X-ray diffraction were obtained by slow diffusion of pentane into a THF solution of **Re-4** at room temperature.

The NMR, IR and UV-visible data for **Re-4** are in agreement with that reported in the literature.⁴

¹H NMR (400 MHz, CD₂Cl₂) δ 8.01 (d, *J* = 8.0 Hz, 2H), 7.92 (t, *J* = 7.9 Hz, 2H), 7.47 (d, *J* = 7.4 Hz, 2H), 3.10 (s, 6H), ppm

¹³C NMR (400 MHz, CD₂Cl₂) δ 163.0, 158.3, 139.4, 126.9, 121.3, 30.4 ppm

IR ν(CO): 2013, 1894, 1881 cm⁻¹

UV-Vis (acetonitrile) λ_{max} (ε) = 315 (6270), 329 (5330), 355 nm (1760 M⁻¹.cm⁻¹)

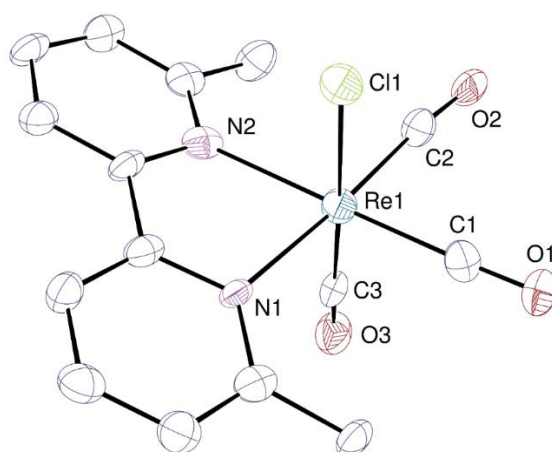
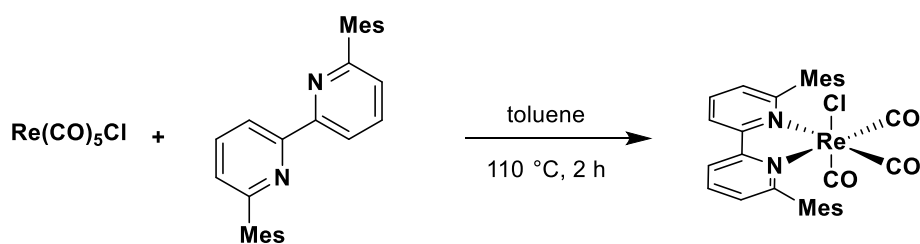


Figure S3: View of **Re-4** with displacement ellipsoids drawn at the 50% probability level and hydrogen atoms omitted.

2.2.2 Synthesis of [Re(6,6'-mesbpy)(CO)₃Cl] **Re-5**



Scheme S2: Synthetic pathway towards [Re(6,6'-mesbpy)(CO)₃Cl] **Re-5**.

Synthesis of 6,6'-dimesityl-2,2'-bipyridine (mesbpy) was performed as previously reported by the Suzuki coupling of 6,6'-dibromo-2,2'-bipyridine with mesitylboronic acid.⁵

[Re(6,6'-mesbpy)(CO)₃Cl] **Re-5** was prepared as follows: in a glovebox, a 50 mL round-bottomed flask equipped with a stirring bar and a *J. Young* valve was charged with 6,6'-dimesityl-2,2'-bipyridine (140 mg, 357 μmol, 1 equiv.), [Re(CO)₅Cl] (130 mg, 359 μmol, 1 equiv.), and 15 mL of anhydrous toluene. The flask was sealed, brought out of the glovebox, and immersed in an oil bath at 110 °C. After 2 hours, the resulting yellow solution was cooled down to room temperature, and the solvent was removed *in vacuo*. The resulting crude yellow solid was purified by column chromatography on silica

gel (DCM:MeOH 99:1). The solid obtained after evaporation of the solvent was suspended in pentane and centrifuged three times for 10 min. The solid was dried under vacuum overnight to give [Re(6,6'-dimesitylbipyridine)(CO)₃Cl] **Re-5** (170 mg, 68%) as a yellow powder. Single crystals suitable for X-ray diffraction were obtained by slow diffusion of pentane into a THF solution of **Re-5** at room temperature.

¹H NMR (400 MHz, CD₂Cl₂) δ 8.29 (d, *J* = 8.3 Hz, 2H), 8.10 (t, *J* = 7.9 Hz, 2H), 7.40 (d, *J* = 7.7 Hz, 2H), 6.98 (s, 4H), 2.34 (s, 6H), 2.15 (s, 6H), 2.00 (s, 6H) ppm

¹³C NMR (400 MHz, CD₂Cl₂) δ 192.3, 190.1, 164.3, 158.0, 139.6, 139.0, 138.7, 136.4, 135.4, 128.9, 128.3, 122.4, 20.9, 20.8, 20.1 ppm

IR ν(CO): 2016, 1918, 1897 cm⁻¹

UV-Vis (acetonitrile) λ_{max} (ε) = 315 (7150), 329 (5940), 370 nm (1400 M⁻¹.cm⁻¹)

Elemental analysis calcd (%) for C₃₁H₂₈ClN₂O₃Re (698.13): C 53.33, H 4.04, N 4.01; found: C 53.60, H 3.88, N 3.97.

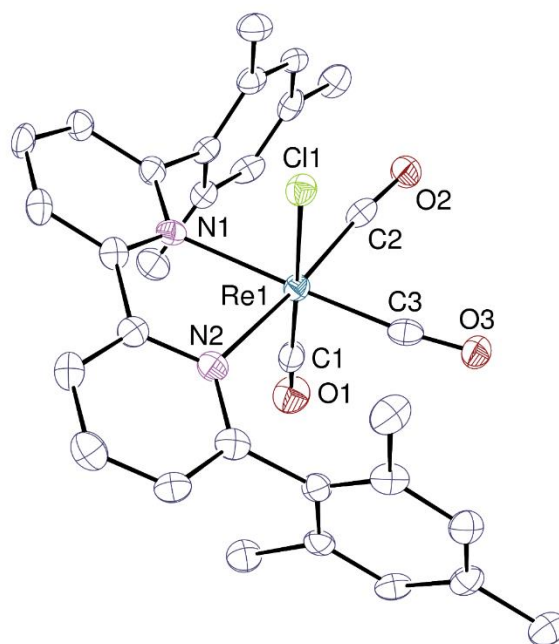


Figure S4: View of **Re-5** with displacement ellipsoids drawn at the 50% probability level and hydrogen atoms omitted.

2.3 Photocatalytic procedures

2.3.1 Photocatalytic reduction of N₂O on NMR scale

The procedure is detailed with photocatalyst [Re(bpy)(CO)₃Cl] **Re-1**. In a glovebox, a 3 mL NMR tube equipped with a *J. Young* valve was charged with [Re(bpy)(CO)₃Cl] **Re-1** (2.3 mg, 5 μmol, 5 mol%), followed by CD₃CN (0.5 mL) and DIPEA (0.1 mL). The tube was sealed and brought out of the glovebox. The reaction mixture was degassed by 3 freeze-pump-thaw cycles and exposed to a N₂O atmosphere (1 bar, ca. 100 μmol, ca. 2.4 mL, 1 equiv.). The tube was then left 2 hours under irradiation using the setup described in Figure S2. The gaseous fraction was sampled using the setup described in Figure S10 and analyzed by GC to determine the N₂ yield.

2.3.2 Photocatalytic reduction of N₂O on a 1.2 mmol scale

The procedure is detailed with photocatalyst [Re(bpy)(CO)₃Cl] **Re-1**. In a glovebox, a Schlenk flask (Figure S5) equipped with two *J. Young* valves, a GC septum (*Supelco*, thermogreen TM LB-2) and a stirring bar was charged with [Re(bpy)(CO)₃Cl] **Re-1** (22.4 mg, 60 μmol, 5 mol%), followed by 6 mL acetonitrile and 1.2 mL DIPEA. The two valves were sealed, and the flask was brought out of the glovebox. The resulting yellow solution was degassed by three freeze-pump-thaw cycles, then exposed to a N₂O atmosphere (1.0 bar, ca. 1.2 mmol, ca. 28.8 mL, 1 equiv.). The flask was left to irradiate in the center of the setup described in Figure S2. At regular intervals valve (*) was opened and 150 μL of the headspace were sampled and analyzed by GC; then, valve (*) was closed.

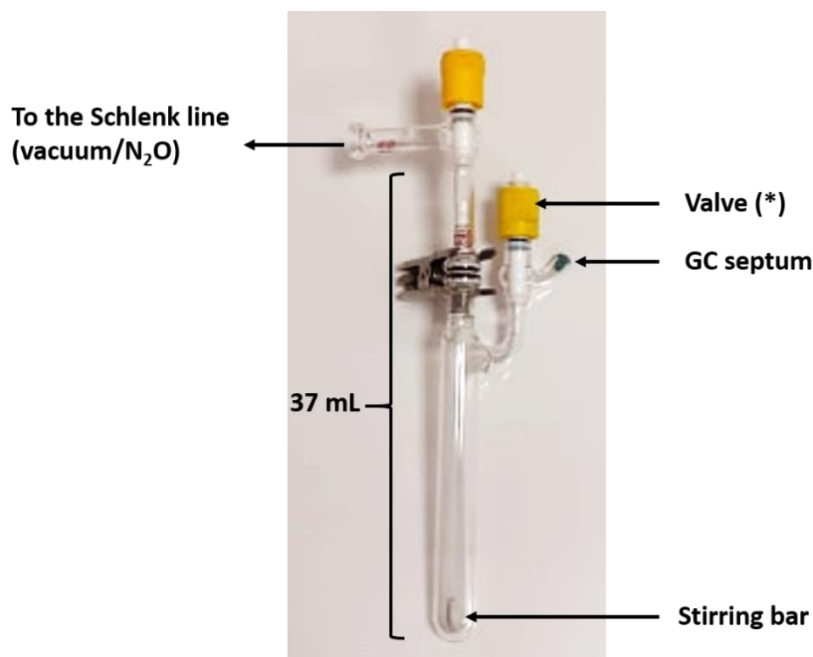


Figure S5: Sideview of the scale-up reaction setup.

TONs for N₂ were calculated as follows:

$$\text{TON} = \frac{n(\text{N}_2)}{n(\text{catalyst})}$$

where $n(\text{N}_2)$ is the final quantity of N₂ in the reaction setup.

The different values of $n(\text{N}_2)$ for each catalyst and corresponding TONs are given in Table S2.

Table S2: Calculation of TON N₂ for each catalyst on 1.2 mmol scale. Reaction conditions: N₂O (1.0 bar, 1.2 mmol), photocatalyst (60 μmol, 5 mol%), CH₃CN (6 mL), DIPEA (1.2 mL).

Entry	Catalyst	TOF ₀ (h ⁻¹)	Time of irradiation (h)	n(N ₂) (mmol)	% N ₂ (TON)
1	Re-1	0.7	22	0.3	22 (5)
2	Re-2	3.7	50	0.84	70 (14)
3	Re-3	4.3	115	1.02	86 (17)
4	Re-4	2.7	100	0.66	55 (11)
5	Re-5	1.1	150	0.73	61 (12)

2.3.3 Photocatalytic reduction of pyridine *N*-oxides

The procedure is detailed in the case of photocatalyst [Re(tbbpy)(CO)₃Cl] **Re-3**:

In a glovebox, a 3 mL NMR tube equipped with a *J. Young* valve was charged with **Re-3** (2.9 mg, 5 mol%), followed by pyridine *N*-oxide (9.5 mg, 100 μmol, 1 equiv.), CD₃CN (0.5 mL), DIPEA (0.1 mL), and mesitylene as an internal standard (10 μL). The tube was sealed, brought out of the glovebox, then left under irradiation using the setup described in Figure S2. The conversion rate and pyridine yield were determined by ¹H NMR integration (protons *ortho* to the nitrogen atom) vs. mesitylene as an internal standard.

Representative NMR spectra for the photocatalytic deoxygenation of pyridine *N*-oxide **1a** with **Re-3** are given in Figure S6. The NMR data for all substituted pyridines are in agreement with those reported in the literature.⁶

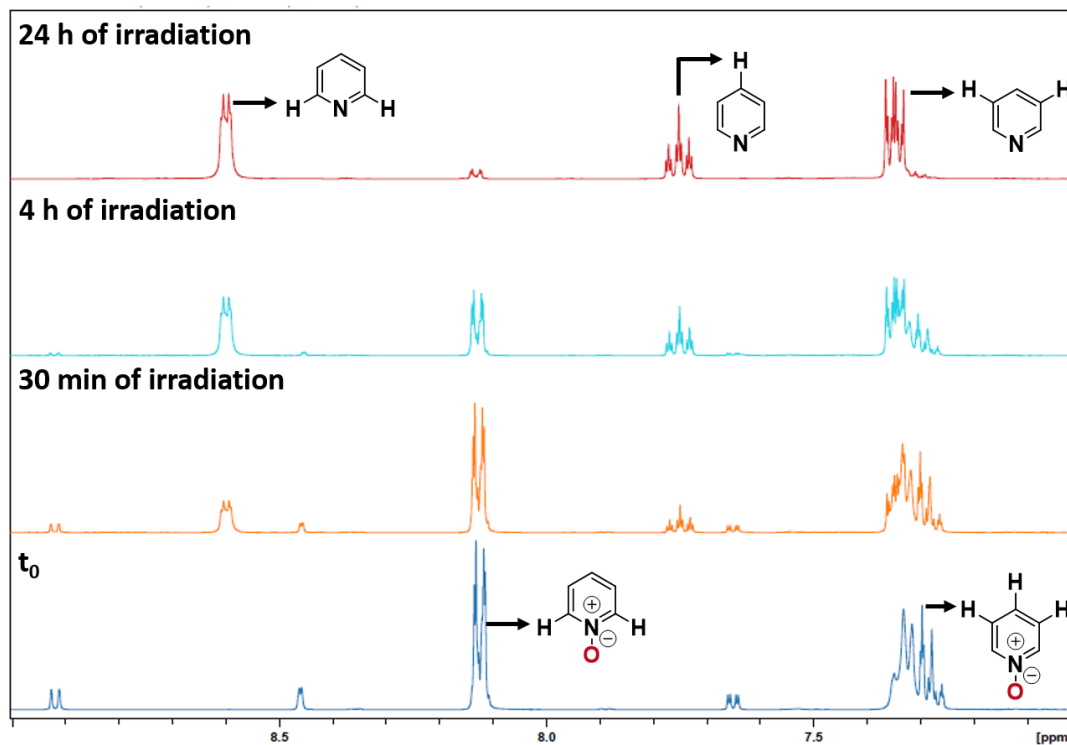
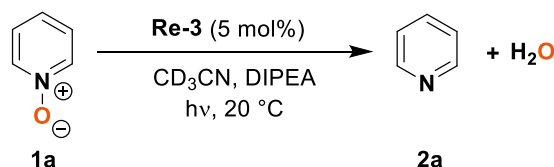


Figure S6: Photocatalytic reduction of pyridine *N*-oxide **1a** with **Re-3**: evolution of the reaction mixture (¹H NMR, aromatic region).

2.3.3.1 Synthesis of 6-methyl-2-(4-octen-4-yl)pyridine from 2-methylpyridine *N*-oxide **4**

2-methylpyridine was oxidized to 2-methylpyridine *N*-oxide according to a reported literature procedure, then was engaged in a nickel-catalyzed hydroheteroarylation with 4-octyne following the procedure reported by Hiyama *et al.*⁷ The product obtained, 6-methyl-2-(4-octen-yl)pyridine *N*-oxide **5** (E/Z: 93/7), was deoxygenated using the following procedure: in a glovebox, a 3 mL NMR tube equipped with a *J. Young* valve was charged with **Re-3** (2.9 mg, 5 μmol, 5 mol%), followed by, 6-methyl-2-(4-octen-yl)pyridine *N*-oxide (21.9 mg, 100 μmol, 1 equiv.), CD₃CN (0.5 mL), DIPEA (0.1 mL), and mesitylene as an internal standard (10 μL). The tube was sealed, brought out of the glovebox, then left under irradiation using the setup described in Figure S2. The conversion rate and pyridine yield were determined by ¹H NMR integration (alkene proton) vs. mesitylene as an internal standard. The reaction afforded 6-methyl-2-(4-octen-4-yl)pyridine **3** in 82% yield after 8 h of irradiation. The NMR data are in agreement with those reported in the literature.⁷

3 GC analyses

3.1 GC conditions

Column: Carboxen 1010 Plot fused silica capillary column (30 m × 0.53 mm × 30 μm); injection temperature: 230 °C; column temperature: 150 °C; flow: 5 mL/min; purge: 2 mL/min; split ratio: 5.0; carrier gas: argon; detector: TCD 230 °C, 30 mA.

3.2 GC calibration

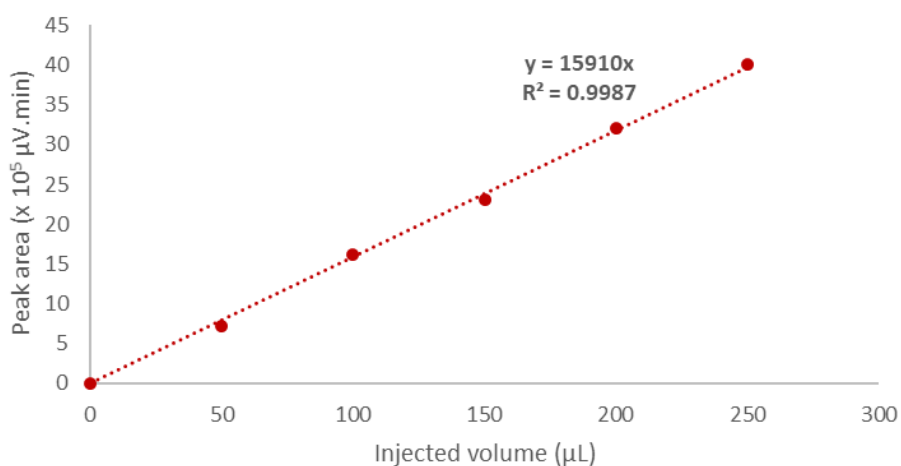


Figure S7: GC Calibration curve for N₂.

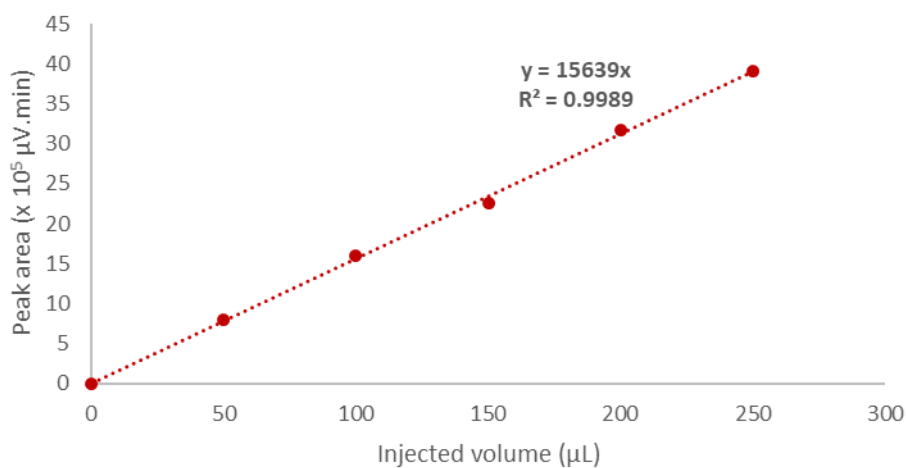


Figure S8: GC Calibration curve for N₂O.

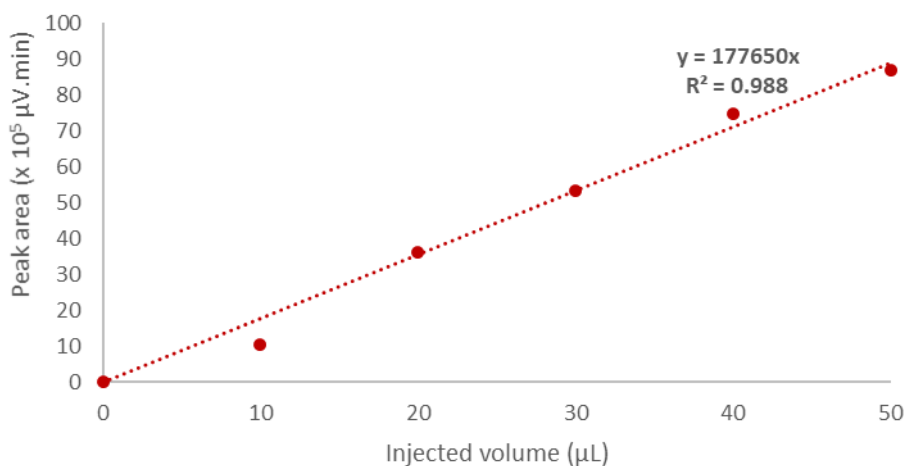


Figure S9: GC Calibration curve for H₂.

Table S3: Retention times and response coefficients of analyzed species.

Species	Retention time (min)	Response factor (μV.min.μL ⁻¹)
H ₂	1.96	177650
N ₂	2.08	15910
N ₂ O	4.45	15639

3.3 Analysis of the gaseous fraction from a J-Young NMR tube

The *J. Young* NMR tube was connected to a small glass chamber, itself connected to the Schlenk line. The chamber was sealed with a GC septum (*Supelco*, thermogreen™ LB-2, Figure S10) and placed under high vacuum ($V = 1 \text{ mL}$, $P = 10^{-2} \text{ mbar}$) to limit air contamination. The chamber was closed, and the *J. Young* NMR tube was open, allowing the gaseous phase to expand. The gas phase was sampled through the septum using a *Hamilton*® *SampleLock* syringe and injected right away into the GC apparatus.

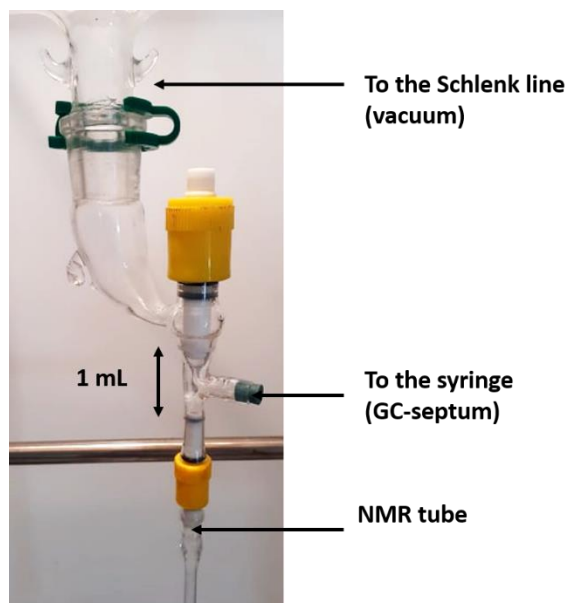


Figure S10: Side view of the apparatus used to analyze the gas phase from a J. Young NMR tube.

Table S4: Results of the control experiments.

Entry	Deviation from standard conditions ^[a]	H ₂ (%) ^[b]	N ₂ (%) ^[b,c]	N ₂ O (%) ^[b]
1	None	1.5	66	32
2	No light	0	4	96
3	No photocatalyst	0	2	98
4	Argon instead of N ₂ O	91	9	0
5	No TEOA	0	8	92
6	DIPEA instead of TEOA	0	76	24

[a] Standard reaction conditions: N₂O (1 bar, 100 μmol), **Re-3** (5 μmol, 5 mol%), CD₃CN (0.5 mL), DIPEA (0.1 mL), 20 °C, 12 h of irradiation. [b] Determined by GC analysis of the gaseous phase. [c] It was impossible to obtain N₂ levels lower than 2 μL in the blank experiments; that residual amount was attributed to contamination by ambient air between sampling and injection for analysis.

4 Analysis data

4.1 Luminescence quenching experiments

For luminescence quenching experiments, a 1 mM solution of the photocatalyst in dry acetonitrile was prepared in a glovebox filled with argon. Out of the glovebox, the photocatalyst was irradiated: at 370 nm for **Re-1**, at 410 nm for **Re-3**. The change of the luminescence upon addition of DIPEA at different concentrations was recorded. These demonstrated that the luminescence was efficiently quenched by DIPEA for both complexes.

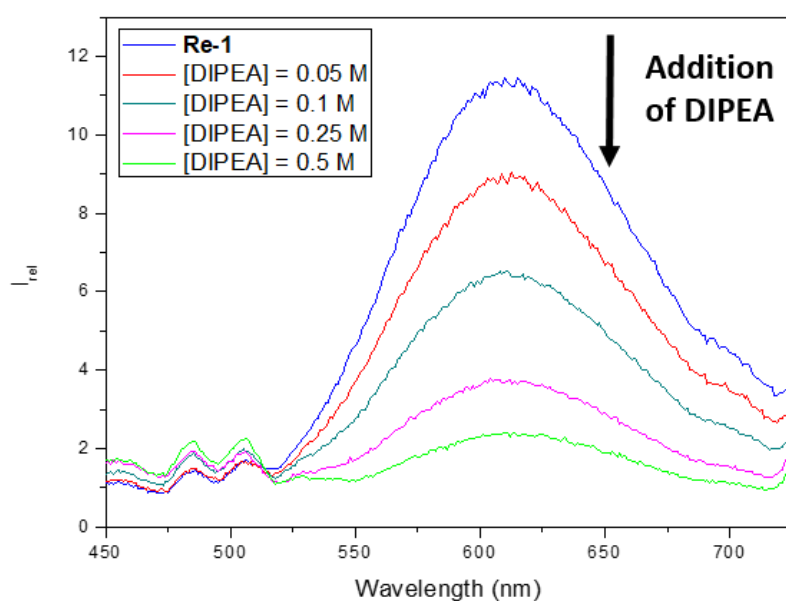


Figure S11: Changes in the luminescence spectra of **Re-1** upon addition of DIPEA at different concentrations in acetonitrile.

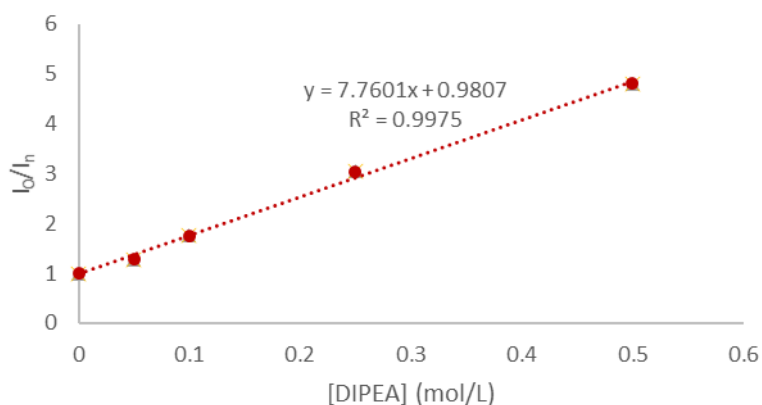


Figure S12: Stern-Volmer quenching of **Re-1** luminescence with DIPEA.

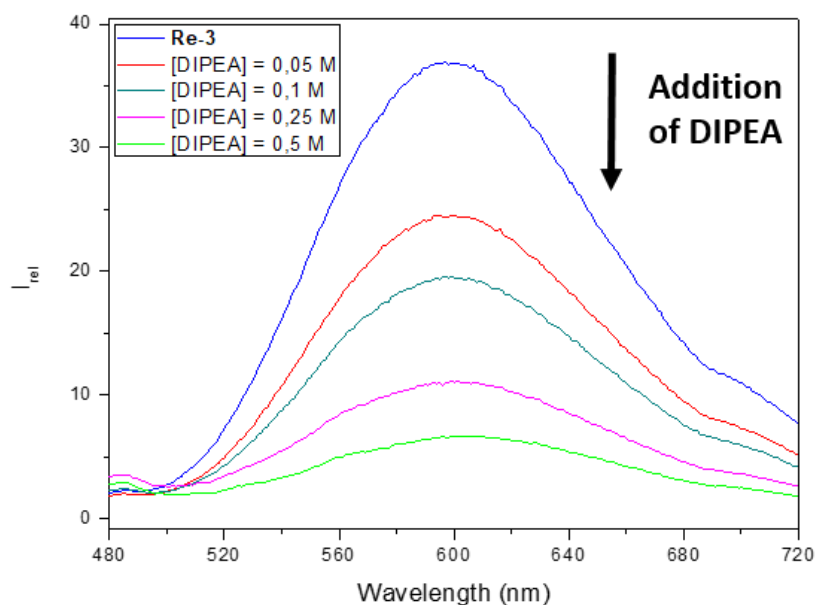


Figure S13: Changes in the luminescence spectra of **Re-3** upon addition of DIPEA at different concentrations in acetonitrile.

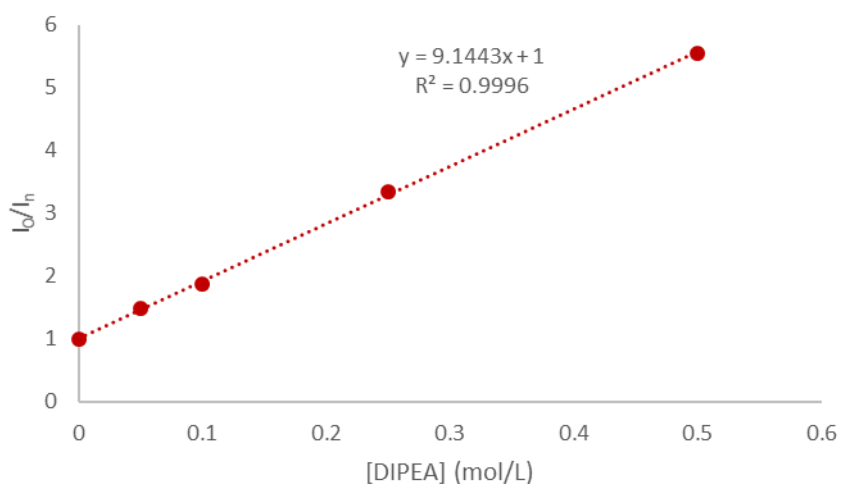


Figure S14: Stern-Volmer quenching of **Re-3** luminescence with DIPEA.

4.2 Crystallography

The data for compound **Re-4**·0.5THF were collected on a *Bruker D8 Quest* diffractometer equipped with an Incoatec Microfocus Source ($I_{\mu S}$ 3.0 Mo) and a PHOTON III area detector, and operated through the APEX3 software,⁸ while those for compound **Re-5**·0.5THF were collected on a Nonius Kappa-CCD area detector diffractometer using graphite-monochromated Mo $K\alpha$ radiation ($\lambda = 0.71073$ Å).⁹ The crystals were mounted either into a glass capillary or on a Mitegen micromount with a

protective coating of Paratone-N oil (Hampton Research). The data were processed with SAINT (**Re-4**) or HKL2000 (**Re-5**).^{10,11} Absorption effects were corrected empirically with the programs SADABS (**Re-4**) or SCALEPACK (**Re-5**).¹¹⁻¹³ All structures were solved by intrinsic phasing with SHELXT,¹⁴ expanded by subsequent difference Fourier synthesis and refined by full-matrix least-squares on F^2 with SHELXL-2014,¹⁵ using the ShelXle interface.¹⁶ All non-hydrogen atoms were refined with anisotropic displacement parameters. The hydrogen atoms were introduced at calculated positions and they were treated as riding atoms with an isotropic displacement parameter equal to 1.2 times that of the parent atom (1.5 for CH₃, with optimized geometry). The solvent THF molecule has twofold rotation symmetry in **Re-4**·0.5THF while that in **Re-5**·0.5THF is disordered around an inversion center and has been given an occupancy parameter of 0.5 accordingly. The molecular plots were drawn with ORTEP-3.¹⁷

Crystal data for compound Re-4·0.5THF. C₁₇H₁₆ClN₂O_{3.5}Re, $M = 525.97$, orthorhombic, space group *Pbcn*, $a = 13.4935(10)$, $b = 22.1756(17)$, $c = 11.2515(8)$ Å, $V = 3366.8(4)$ Å³, $Z = 8$, $D_c = 2.075$ g cm⁻³, $\mu = 7.399$ mm⁻¹, $F(000) = 2016$. Refinement of 224 parameters on 3201 independent reflections out of 41305 measured reflections ($R_{\text{int}} = 0.051$) led to $R_1 = 0.052$, $wR_2 = 0.114$, $S = 1.506$, $\Delta\rho_{\text{min}} = -2.09$, $\Delta\rho_{\text{max}} = 1.91$ e Å⁻³.

Crystal data for compound Re-5·0.5THF. C₃₃H₃₂ClN₂O_{3.5}Re, $M = 734.25$, monoclinic, space group *C2/c*, $a = 35.2615(16)$, $b = 8.1575(3)$, $c = 22.7433(10)$ Å, $\beta = 116.166(3)^\circ$, $V = 5871.6(5)$ Å³, $Z = 8$, $D_c = 1.661$ g cm⁻³, $\mu = 4.269$ mm⁻¹, $F(000) = 2912$. Refinement of 394 parameters on 5550 independent reflections out of 155149 measured reflections ($R_{\text{int}} = 0.065$) led to $R_1 = 0.030$, $wR_2 = 0.061$, $S = 1.101$, $\Delta\rho_{\text{min}} = -1.01$, $\Delta\rho_{\text{max}} = 1.66$ e.Å⁻³.

4.3 Copies of NMR spectra

4.3.1 Re-4

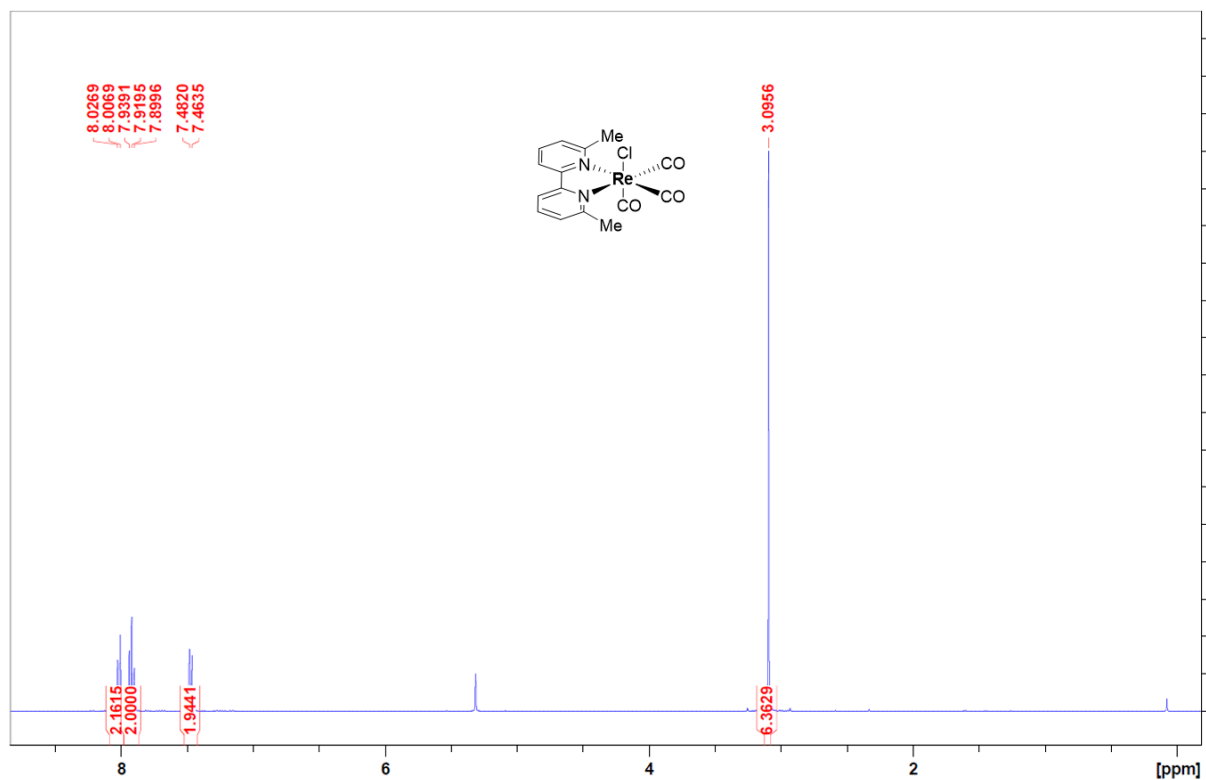


Figure S15: ^1H NMR spectrum of **Re-4** in CD_2Cl_2 .

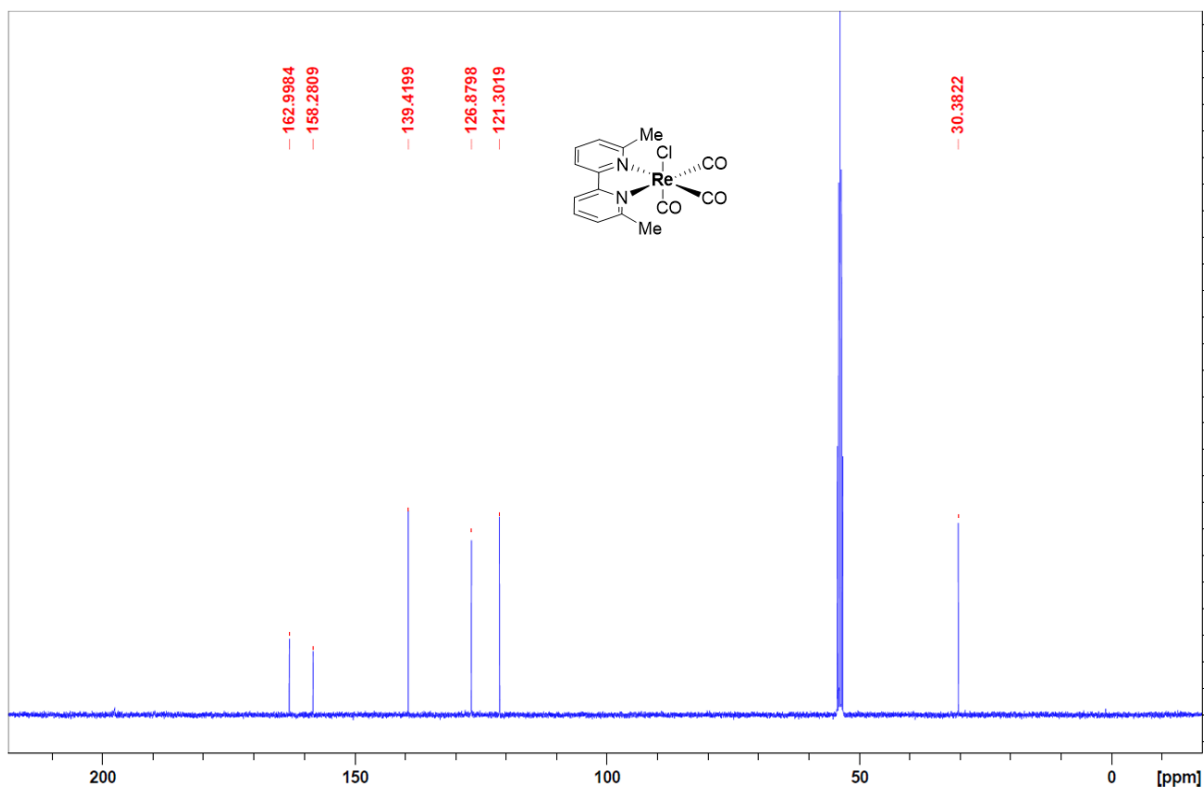


Figure S16: ^{13}C NMR spectrum of **Re-4** in CD_2Cl_2 .

4.3.2 Re-5

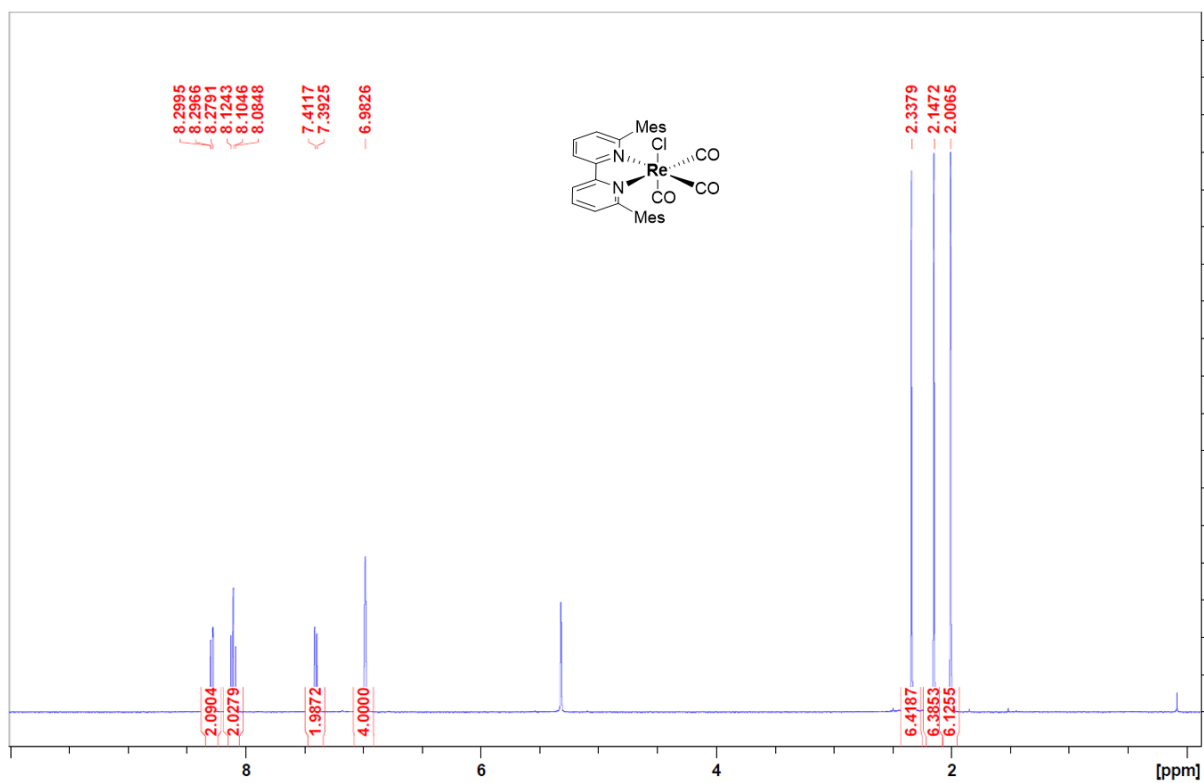


Figure S17: ^1H NMR spectrum of **Re-5** in CD_2Cl_2 .

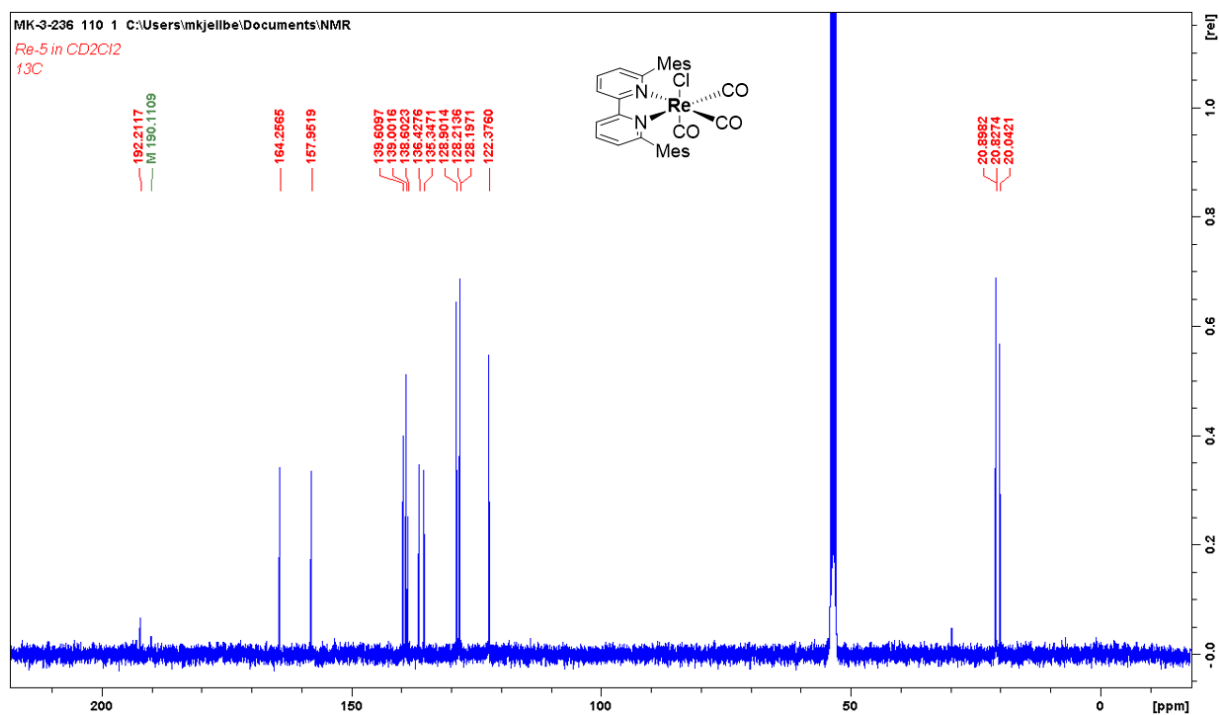


Figure S18: ¹³C NMR spectrum of Re-5 in CD₂Cl₂.

4.4 Copies of GC traces

4.4.1 Representative GC traces for the photocatalyzed reduction of N₂O by Re-3

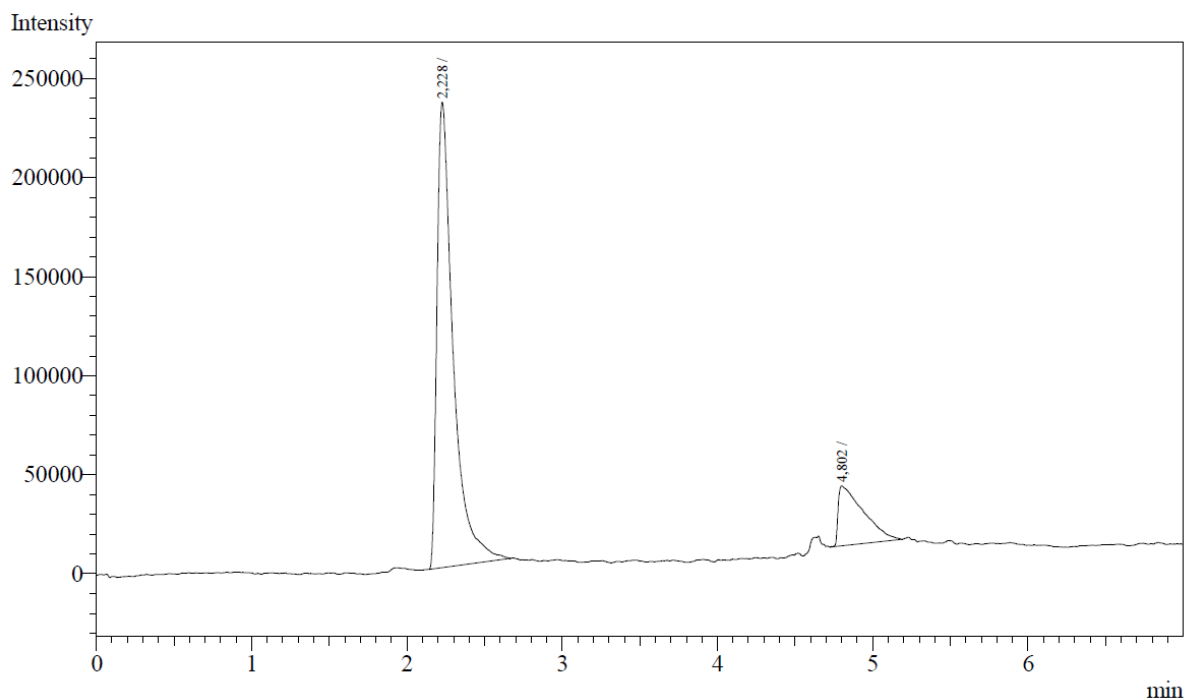


Figure S19: GC analysis of the gaseous phase after 24 h of irradiation, on NMR scale.

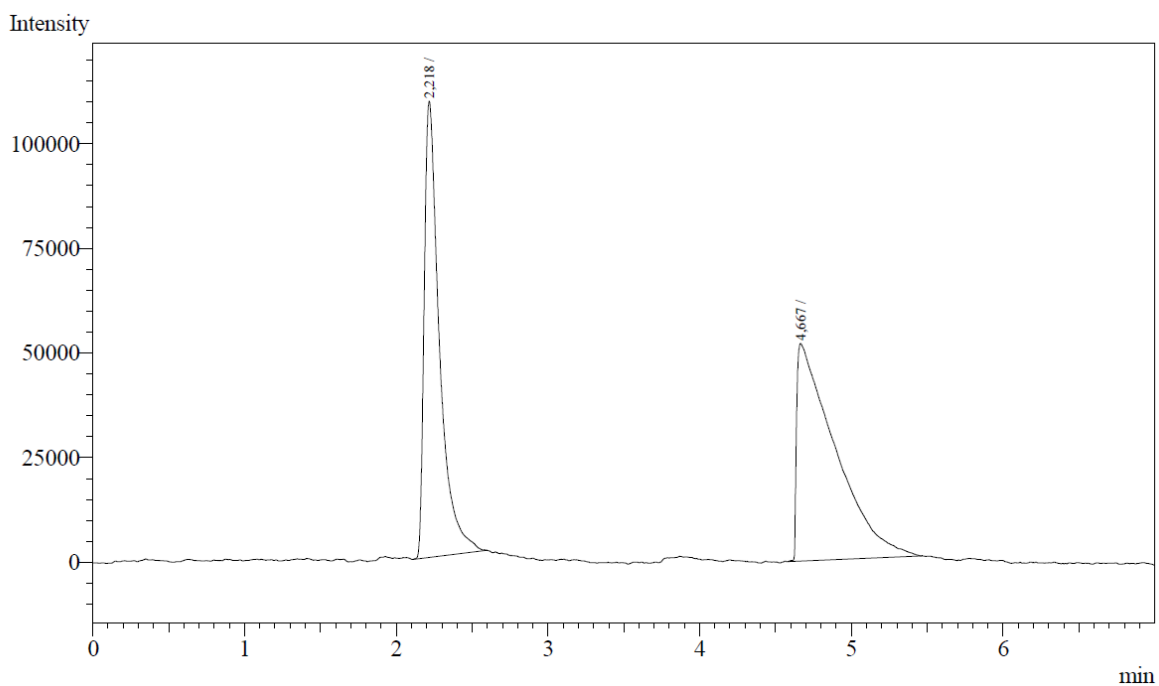


Figure S20: GC analysis of the gaseous phase after 5 h of irradiation, on a 1.2 mmol scale.

4.4.2 GC trace for the reduction of N_2O catalyzed by **Re-1** in presence of TEOA

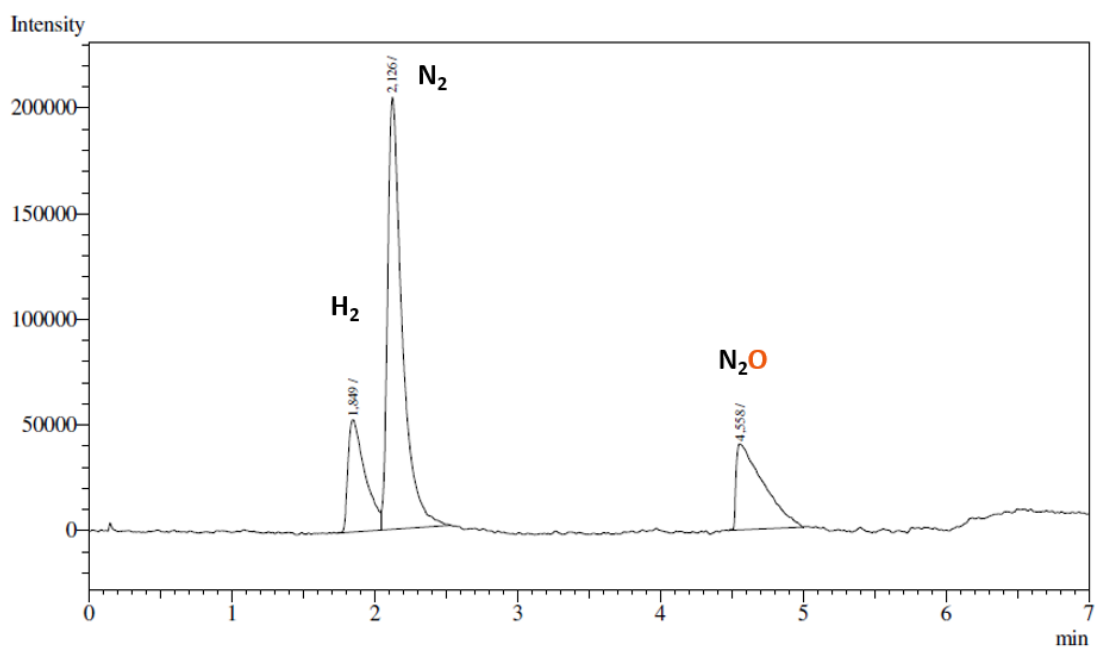


Figure S21: GC analysis of the gaseous phase after 2 h of irradiation.

4.4.3 GC traces for the control experiments for the photoreduction of N_2O with **Re-1** (see Table 1)

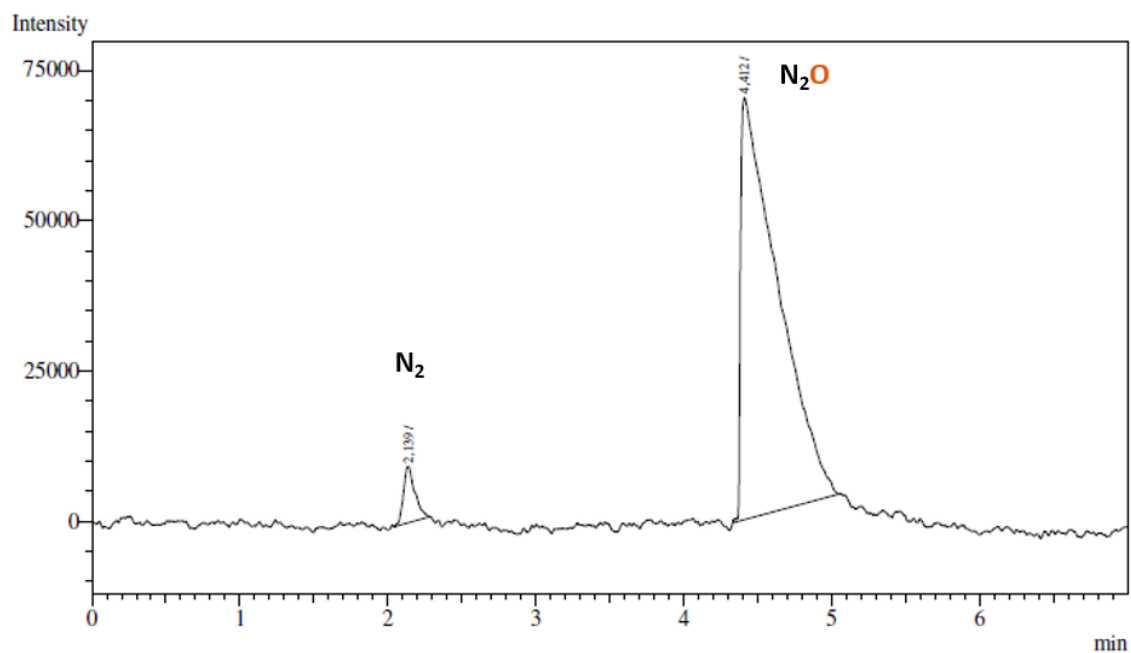


Figure S22: Control experiment without light.

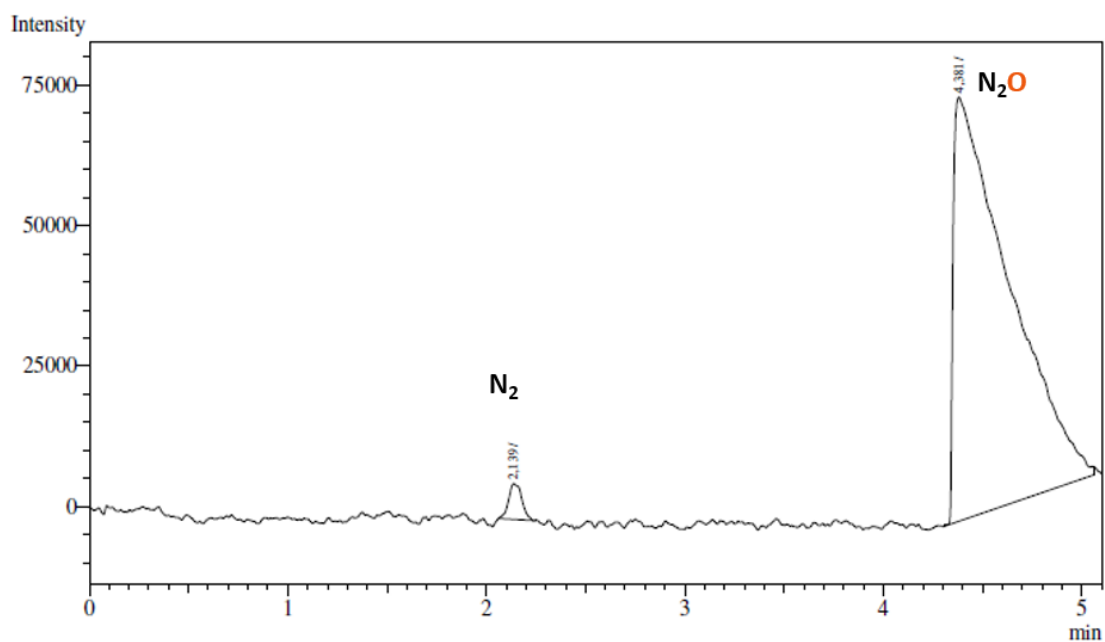


Figure S23: Control experiment without **Re-1**.

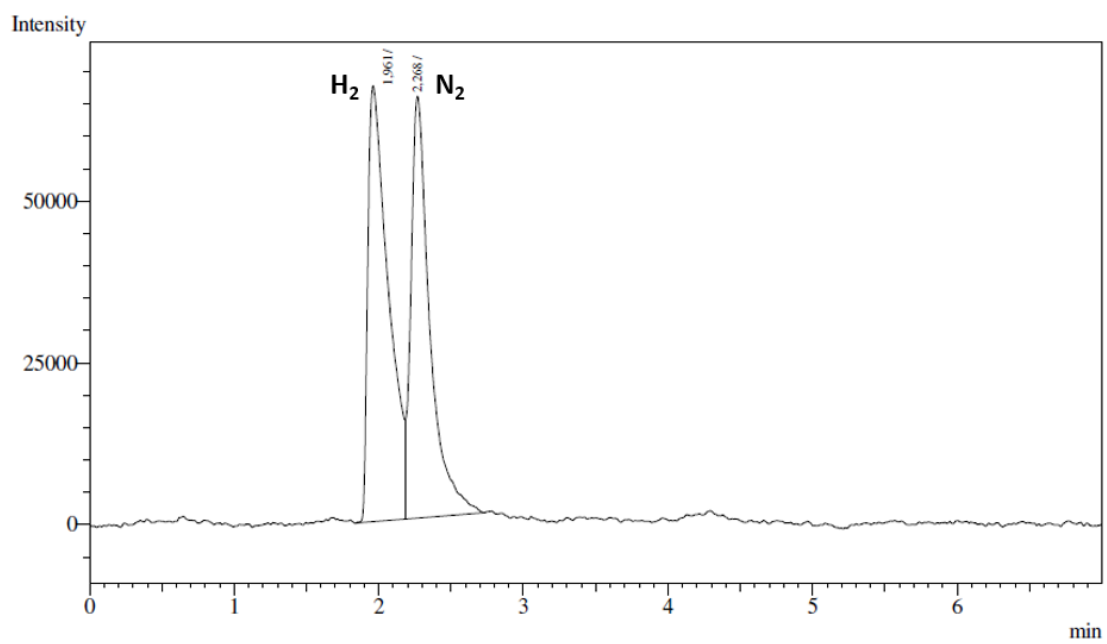


Figure S24: Control experiment with Ar instead of N₂O.

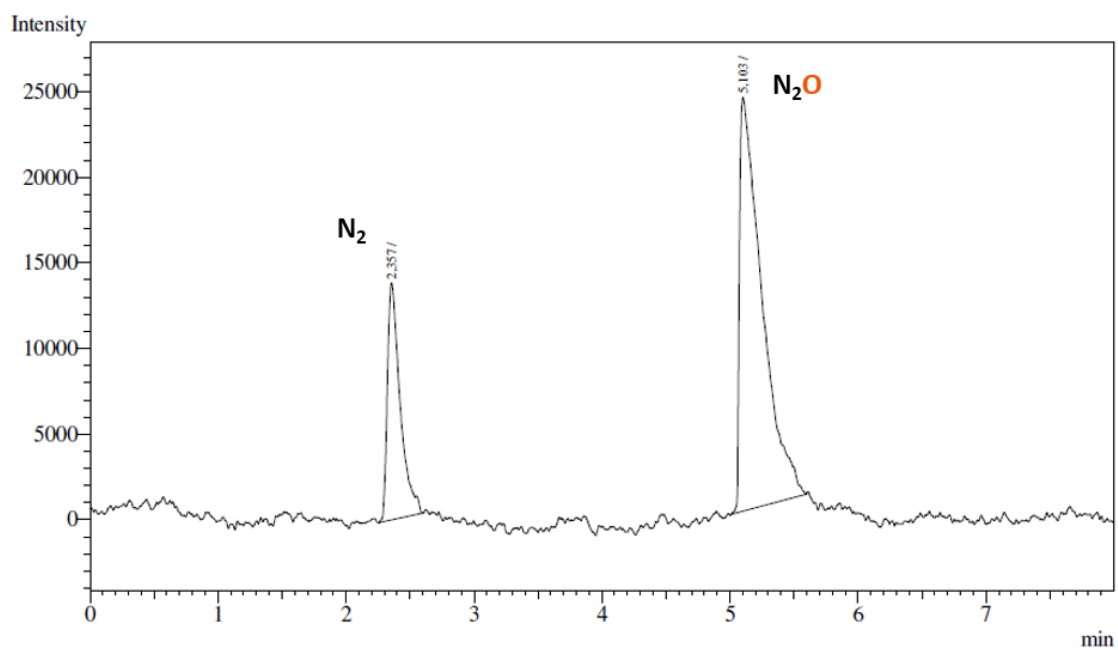


Figure S25: Control experiment without TEOA.

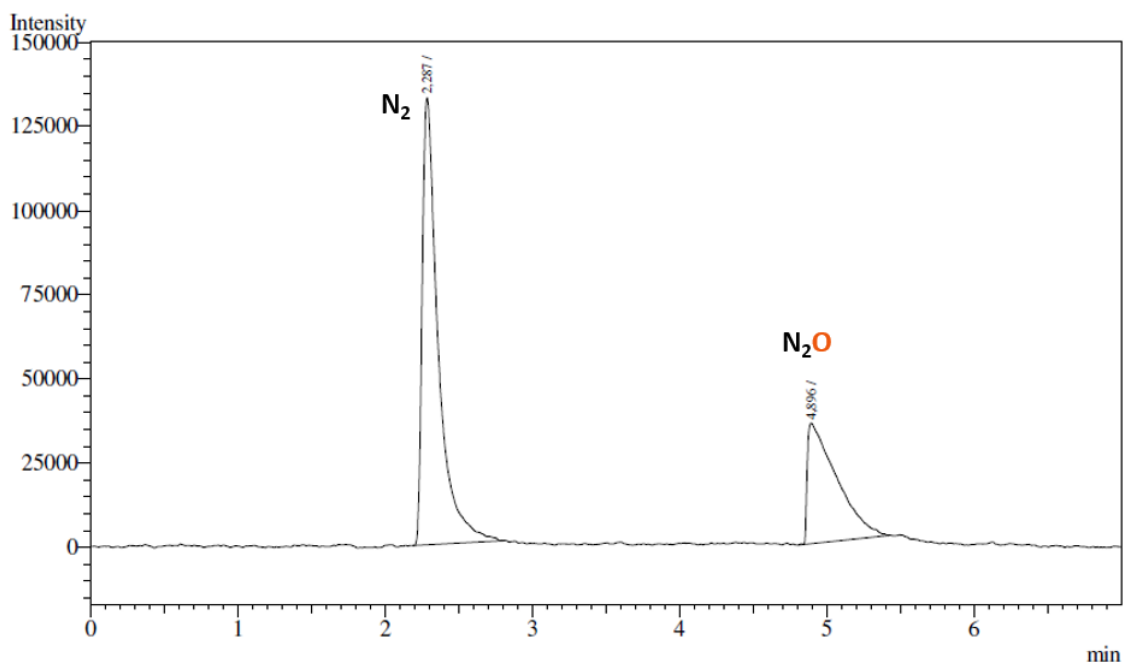


Figure S26: Control experiment with DIPEA instead of TEOA.

4.5 Copies of UV-Vis spectra

4.5.1 Absorption spectrum of Re-4

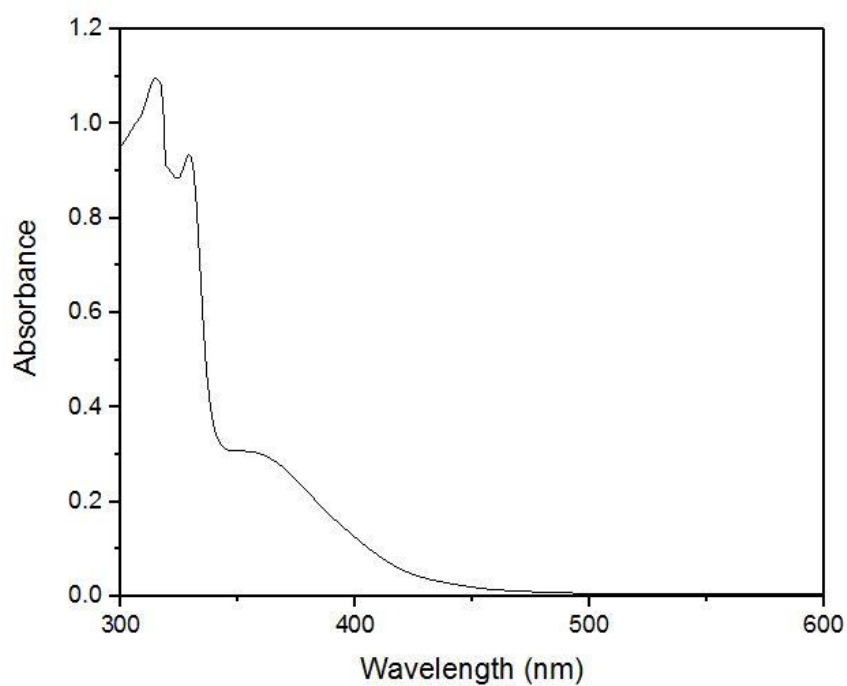


Figure S27: Absorption spectrum of Re-4 (175 μ M in acetonitrile) at 293 K.

4.5.2 Absorption spectrum of **Re-5**

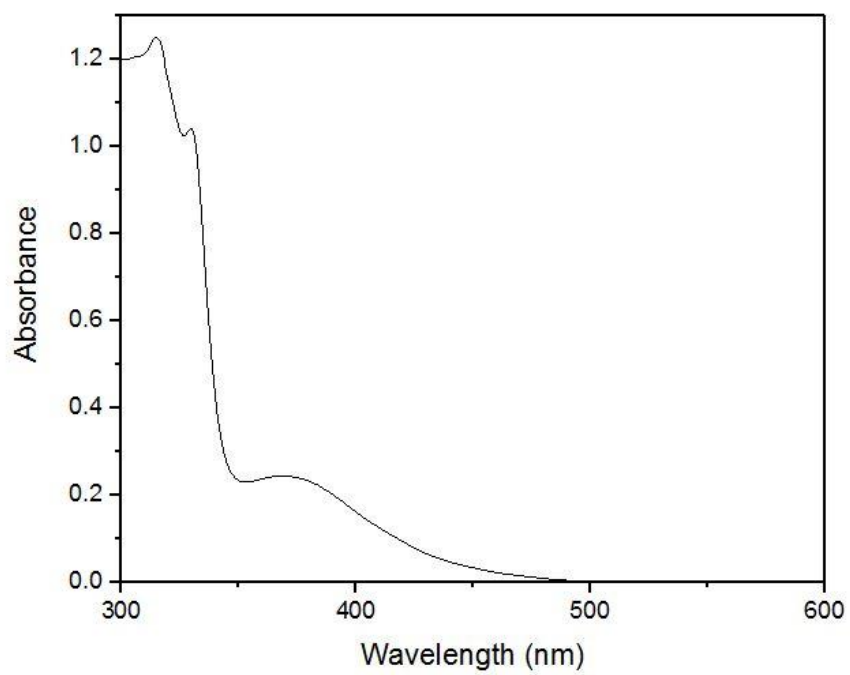


Figure S28: Absorption spectrum of **Re-5** (175 μ M in acetonitrile) at 293 K.

5 References

- 1 Hori, H., Ishihara, J., Koike, K., Takeuchi, K., Ibusuki, T. & Ishitani, O. Photoinduced Formation of [fac-Re(bpy)(CO)₃CN] from [fac-Re(bpy)(CO)₃(4-CNpy)]⁺ (bpy = 2,2'-bipyridine, py = pyridine): CN Group Rearrangement of a Cyanopyridine Ligand onto Central Metal. *Chem. Lett.* **26**, 1249-1250 (1997).
- 2 Gibson, D. H., Yin, X., He, H. & Mashuta, M. S. Synthesis and Reactions of fac-[Re(dmbpy)(CO)₃X] (dmbpy = 4,4'-Dimethyl-2,2'-bipyridine; X = COOH, CHO) and Their Derivatives. *Organometallics* **22**, 337-346 (2003).
- 3 Smieja, J. M. & Kubiak, C. P. Re(bipy-tBu)(CO)₃Cl-improved Catalytic Activity for Reduction of Carbon Dioxide: IR-Spectroelectrochemical and Mechanistic Studies. *Inorg. Chem.* **49**, 9283-9289 (2010).
- 4 Adams, F., Pschenitzka, M. & Rieger, B. Yttrium-Catalyzed Synthesis of Bipyridine-Functionalized AB-Block Copolymers: Micellar Support for Photocatalytic Active Rhenium-Complexes. *ChemCatChem* **10**, 4309-4316 (2018).
- 5 Schmittel, M., Ganz, A., Schenk, W. A. & Hagel, M. Synthesis and Coordination Properties of 6,6'-Dimesityl-2,2'-bipyridine. *Zeitschrift für Naturforschung B* **54**, 559-564 (1999).
- 6 Spectral Database for Organic Compounds (SDBS); <http://sdb.sdb.aist.go.jp/sbds/> (accessed July 29 2020). SDBS No. 518, 1824, 9994, 10015, 9996, and 5723
- 7 Kanyiva, K. S., Nakao, Y. & Hiyama, T. Nickel-Catalyzed Addition of Pyridine-N-oxides across Alkynes. *Angew. Chem. Int. Ed.* **46**, 8872-8874 (2007).
- 8 APEX3 v. 2019.1-0 (Bruker AXS, Madison, Wisconsin, USA, 2019).
- 9 COLLECT (Nonius BV, The Netherlands, 1998).
- 10 SAINT v. 8.40A (Bruker Nano, Madison, Wisconsin, USA, 2019).
- 11 Otwinowski, Z. & Minor, W., [20] Processing of X-ray diffraction data collected in oscillation mode in *Methods Enzymol.* Vol. 276 307-326 (Academic Press, 1997).
- 12 SADABS v. 2016/2 (Bruker AXS, Madison, Wisconsin, USA, 2016).
- 13 Krause, L., Herbst-Irmer, R., Sheldrick, G. M. & Stalke, D. Comparison of silver and molybdenum microfocus X-ray sources for single-crystal structure determination. *J. Appl. Crystallogr.* **48**, 3-10 (2015).
- 14 Sheldrick, G. SHELXT - Integrated space-group and crystal-structure determination. *Acta Crystallographica Section A* **71**, 3-8 (2015).
- 15 Sheldrick, G. Crystal structure refinement with SHELXL. *Acta Crystallographica Section C* **71**, 3-8 (2015).
- 16 Hubschle, C. B., Sheldrick, G. M. & Dittrich, B. ShelXle: a Qt graphical user interface for SHELXL. *J. Appl. Crystallogr.* **44**, 1281-1284 (2011).
- 17 Farrugia, L. WinGX and ORTEP for Windows: an update. *J. Appl. Crystallogr.* **45**, 849-854 (2012).

ESI.pdf (2.61 MiB)

[view on ChemRxiv](#) • [download file](#)

Other files

Re-4.cif (1.55 MiB)

[view on ChemRxiv](#) • [download file](#)

Re-5.cif (576.06 KiB)

[view on ChemRxiv](#) • [download file](#)
